University of Illinois at Urbana-Champaign

ACRC

Air Conditioning and Refrigeration Center A National Science Foundation/University Cooperative Research Center

Study of Multilouvered Heat Exchangers at Low Reynolds numbers

D. K. Tafti, X. Zhang, and D. Guo

ACRC TR-229 May 2004

For additional information:

Air Conditioning and Refrigeration Center
University of Illinois
Mechanical & Industrial Engineering Dept.
1206 West Green Street
Urbana, IL 61801

(217) 333-3115

Prepared as part of ACRC Project #139
Study of Multilouvered Heat Exchangers at Low Reynolds Numbers
D. K. Tafti, Principal Investigator

The Air Conditioning and Refrigeration Center was founded in 1988 with a grant from the estate of Richard W. Kritzer, the founder of Peerless of America Inc. A State of Illinois Technology Challenge Grant helped build the laboratory facilities. The ACRC receives continuing support from the Richard W. Kritzer Endowment and the National Science Foundation. The following organizations have also become sponsors of the Center.

Alcan Aluminum Corporation
Amana Refrigeration, Inc.
Arçelik A. S.
Behr GmbH and Co.
Carrier Corporation
Copeland Corporation
Daikin Industries, Ltd.
Delphi Thermal and Interior
Embraco S. A.
Fujitsu General Limited
General Motors Corporation
Hill PHOENIX
Honeywell, Inc.
Hydro Aluminum Adrian, Inc.
Ingersoll-Rand Company
Lennox International, Inc.
LG Electronics, Inc.
Modine Manufacturing Co.
Parker Hannifin Corporation
Peerless of America, Inc.
Samsung Electronics Co., Ltd.
Sanyo Electric Co., Ltd.
Tecumseh Products Company
Trane
Visteon Automotive Systems
Wieland-Werke, AG
Wolverine Tube, Inc.

For additional information:

Air Conditioning & Refrigeration Center
Mechanical & Industrial Engineering Dept.
University of Illinois
1206 West Green Street
Urbana, IL 61801

217 333 3115

Table of Contents

List of Figures

Page

List of Tables

Page

Chapter 1. Flow Efficiency

Abstract

The paper studies the effect of Reynolds number, fin pitch, louver thickness, and louver angle on flow efficiency in multi-louvered fins. Results show that flow efficiency is strongly dependent on geometrical parameters, especially at low Reynolds numbers. Flow efficiency increases with Reynolds number and louver angle, while decreasing with fin pitch and thickness ratio. A characteristic flow efficiency length scale ratio is identified based on geometrical and first-order hydrodynamic effects, which together with numerical results is used to develop a general correlation for flow efficiency. Comparisons show that the correlation represents more than 95% of numerical predictions within a 10% error band, and 80% of predictions within a 5% error band over a wide range of geometrical and hydrodynamic conditions.

Nomenclature

b	non-dimensional fin thickness (b^* / L_P^*),
d	characteristic flow efficiency length scale ratio,
D_h	non-dimensional hydraulic diameter,
f	friction factor,
F_p	non-dimensional fin pitch (F_p^* / L_p^*),
F_d	non-dimensional flow depth,
k	thermal conductivity,
L_p^*	dimensional louver pitch (characteristic length scale), $L_p = 1$,
Nu	non-dimensional heat transfer coefficient, $Nu = \dfrac{h^* L_p^*}{k} = \dfrac{-\partial T / \partial n}{(1 - T_{ref})}$,
Re	Reynolds number, $\mathrm{Re}_{in} = u_{in}^* L_p^* / \nu$, $\mathrm{Re}_{L_P} = V_c^* L_p^* / \nu$,
T_{ref}	Mixed mean temperature,
u	Streamwise velocity (in x- direction),
v	Cross-stream velocity (in y- direction),
u_{in}^*	dimensional inlet velocity (characteristic velocity scale),
V_c	Average velocity at minimum cross-sectional area,
x	streamwise direction,
y	cross-stream direction.

Greek symbols

η	flow efficiency, $\eta = \dfrac{\alpha_{mean}}{\theta}$,
θ	degrees, louver angle,
α	degrees, flow angle, $\alpha = \tan^{-1} \dfrac{\int v dx / L_P}{\int u dy / F_P}$,
ν	kinematic viscosity,

Superscripts

*	dimensional quantities

Subscripts

F	based on fin,
L	based on louver
c	critical

1.1. Introduction

Compact heat exchangers are used in a variety of automotive, residential air-conditioning and refrigeration applications. For air-side heat transfer augmentation, multilouvered fins are quite popular. Beauvais [1] was the first to conduct flow visualization experiments on the louvered fin array. He demonstrated that louvers, rather than acting as surface roughness that enhanced heat transfer performance, acted to realign the airflow in the direction parallel to themselves. Davenport [2] performed flow visualization experiments identical to those of Beauvais and further demonstrated two flow regimes, duct directed flow, and louver directed flow. In general, the flow direction follows the path of least hydraulic resistance. Under certain conditions, one of them being low Reynolds number, the flow has a propensity to move straight through between fins, rather than align itself to the louvers. At low Reynolds numbers, this is a result of the high flow resistance between louvers brought about by the thick boundary layers.

The flow direction has profound implications on the overall heat capacity of the fin by virtue of its strong effect on the heat transfer coefficient. It is particularly crucial for low Reynolds number applications (Re < 500), in which the natural tendency for air is to flow straight through the fin and not over the louvers. Hence, it is important to be able to quantify and predict the flow direction.

Flow efficiency (η) is used to describe the percentage of the fluid flowing along the louver direction. A 100% efficiency represents ideal louver directed flow while 0% represents complete duct directed flow. In the past, two kinds of definitions of flow efficiency have been used. In experimental dye injection studies [3-6] flow efficiency is defined as the ratio of actual transverse distance (N) traveled by the dye to the ideal distance (D) if the flow were aligned with the louver.

$$\eta_{\exp} = \frac{N}{D}$$

In numerical simulations, because the flow angle can be easily obtained for each individual louver, flow efficiency is defined to be the ratio of mean flow angle (α_{mean}), which is obtained by averaging flow angles through out the louver bank (inlet, redirection and exit louvers are not included), to louver angle (θ) as follows:

$$\eta = \frac{\alpha_{mean}}{\theta}$$

In the present paper, the average velocity ratio (the average normal velocity across top boundary to that across the left boundary) is used to define flow angle in an individual block surrounding a louver, as follows[1]:

$$\alpha = \tan^{-1}\frac{\int v dx / L_P}{\int u dy / F_P}$$

For a small louver angle (θ<30), the difference between $\eta_{\exp}$ and η is small[2].

Webb and Trauger (hereafter referred to as WT) [3] experimentally studied the flow structure in multilouvered fin geometries for six fin pitch ratios (0.7 to 1.5), one thickness ratio (0.0423) and two louver angles (20 and 30 degrees). Reynolds number (based on louver pitch) ranged from 400 to 4000. Their results showed that flow efficiency increased with increasing Reynolds number until a critical Reynolds number was reached,

$$\mathrm{Re}_{W,c} = 828\left(\frac{\theta}{90}\right)^{-0.34}, \tag{1}$$

Before the critical value, flow efficiency depends on, and increases with Reynolds number, louver angle, and decreases with fin pitch ratio.

$$\eta_W = 0.091\mathrm{Re}^{\,0.39}\left(\frac{L_p}{F_p}\right)^{0.44}\left(\frac{\theta}{90}\right)^{0.3} \tag{2}$$

Beyond the critical value, flow efficiency is only affected by fin pitch ratio.

$$\eta_{w,\max} = 0.95\left(\frac{L_p}{F_p}\right)^{0.23} \tag{3}$$

The above flow efficiency is not continuous at the critical Reynolds number. To remedy this deficiency, eqn. (2) was modified by Sahnoun and Webb (hereafter referred to as SW) [4] to keep the flow efficiency continuous at the critical Reynolds number:

$\eta_W = 0.95\left(\frac{L_p}{F_p}\right)^{0.23} - 0.00003717\times\left[828\left(\frac{2\theta}{\pi}\right)^{-0.34} - \mathrm{Re}\right]^{1.1}\left(\frac{L_p}{F_p}\right)^{-1.35}\left(\frac{2\theta}{\pi}\right)^{-0.61}$. It is interested to note that in SW's correlation, the critical Reynolds number depends only on louver angle while the flow efficiency beyond this Reynolds number depends only on fin pitch ratio.

---

[1] The flow angle (α) has also been defined as the ratio of mass flow rates: $\alpha_A = \tan^{-1}\left(\int_0^{L_P} v dx / \int_0^{F_P} u dy\right)$. This definition is inconsistent for $F_p \neq 1$. For example when the flow is louver directed ($v = u\tan(\theta)$),

$\alpha_A = \tan^{-1}\left[\frac{L_P}{F_P}\tan(\theta)\right] \neq \theta$.

[2] $\eta_{\exp} = \frac{N}{D} = \frac{\tan(\alpha_{mean})}{\tan(\theta)} \approx \frac{\alpha_{mean}}{\theta} = \eta$.

Achaichia and Cowell (hereafter referred to as AC) [7] used numerical calculations to model the flow through a simplified two-dimensional louver array. The louvers were assumed to be infinitely thin, and the flow to be fully developed. The fully-developed assumption and zero thickness will overpredict the flow efficiency, particularly as the louver angle decreases and the fin pitch increases. In these geometries, there is a "development length" for flow efficiency before it achieves its "fully-developed" value. AC's simulations do not resolve this. From their numerical simulations, the following correlation for flow efficiency was given:

$$\eta_A = (0.936 - 243/\mathrm{Re} - 1.76\frac{F_p}{L_p} + 0.995\theta)/\theta \,. \tag{4}$$

As Reynolds number tends to infinity, flow efficiency in equation (4) approaches an asymptotic value depending on fin pitch ratio and louver angle:

$\eta_{A,\max} = (0.936 - 1.76\frac{F_p}{L_p} + 0.995\theta)/\theta$. The critical Reynolds number for $\frac{\eta_A}{\eta_{A,\max}} = 0.95$ is:

$$\mathrm{Re}_{A,c} = \frac{4860}{(0.936 - 1.76(F_P/L_P) + 0.995\theta)} \,.$$

In 1996, Bellows (hereafter referred to as B) [5] conducted flow visualization experiments and investigated the effect of fin pitch ratio and louver angle on flow efficiency. Using AC's correlation as a starting point, and taking into consideration developing flow effects, a general correlation was developed as:

$$\eta_B = (-5 - 300/\mathrm{Re} - 10\frac{F_p}{L_p} + 1.34\theta)/\theta \quad . \tag{5}$$

The asymptotic flow efficiency as Reynolds number tends to infinity is:

$\eta_{B,\max} = (-5 - 10\frac{F_p}{L_p} + 1.34\theta)/\theta$ and the critical Reynolds number for $\frac{\eta_B}{\eta_{B,\max}} = 0.95$ is:

$$\mathrm{Re}_{B,c} = \frac{6000}{(-5 - 10(F_P/L_P) + 1.34\theta)} \,.$$

To summarize, flow efficiency is a function of Reynolds number and geometrical parameters, fin pitch ratio and louver angle at low and intermediate Reynolds number. Flow efficiency increases with increase of Reynolds number and louver angle, and decreases with fin pitch ratio. As Reynolds number increases, flow undergoes a transition from duct directed flow (low efficiency) to louver directed flow (high efficiency). There exists a critical Reynolds number beyond which the flow efficiency is independent of Reynolds number. All previous correlations agree in predicting the general trends. However, substantial quantitative differences exist.

Figure 1.1 (a) plots the critical Reynolds numbers from previous correlations. SW's values are much higher than that of AC's and B', especially at large louver angle. On the other hand, the difference between B and AC is small. Fin pitch ratio has a small effect on critical Reynolds number at large louver angle. Figure 1.1 (b) plots the asymptotic flow efficiency from these correlations. B's results show the strongest dependence on both fin pitch ratio and louver angle, whereas the least is shown in SW's results. As fin pitch increases to 1.5, the flow efficiency in

SW's results can be more than 2 times larger than that in B's at θ=20. In Figure 1.1 (c), contrary to other results, flow efficiency in WT's experiments shows a near linear increase in flow efficiency with the Reynolds number (concave curve with log scale), during the transition from duct to louver directed flow. Figure 1.1 (c) also shows that, before modification, WT's results show better agreement with others at very low Reynolds number, whereas results of SW and WT agree better beyond Reynolds number 50.

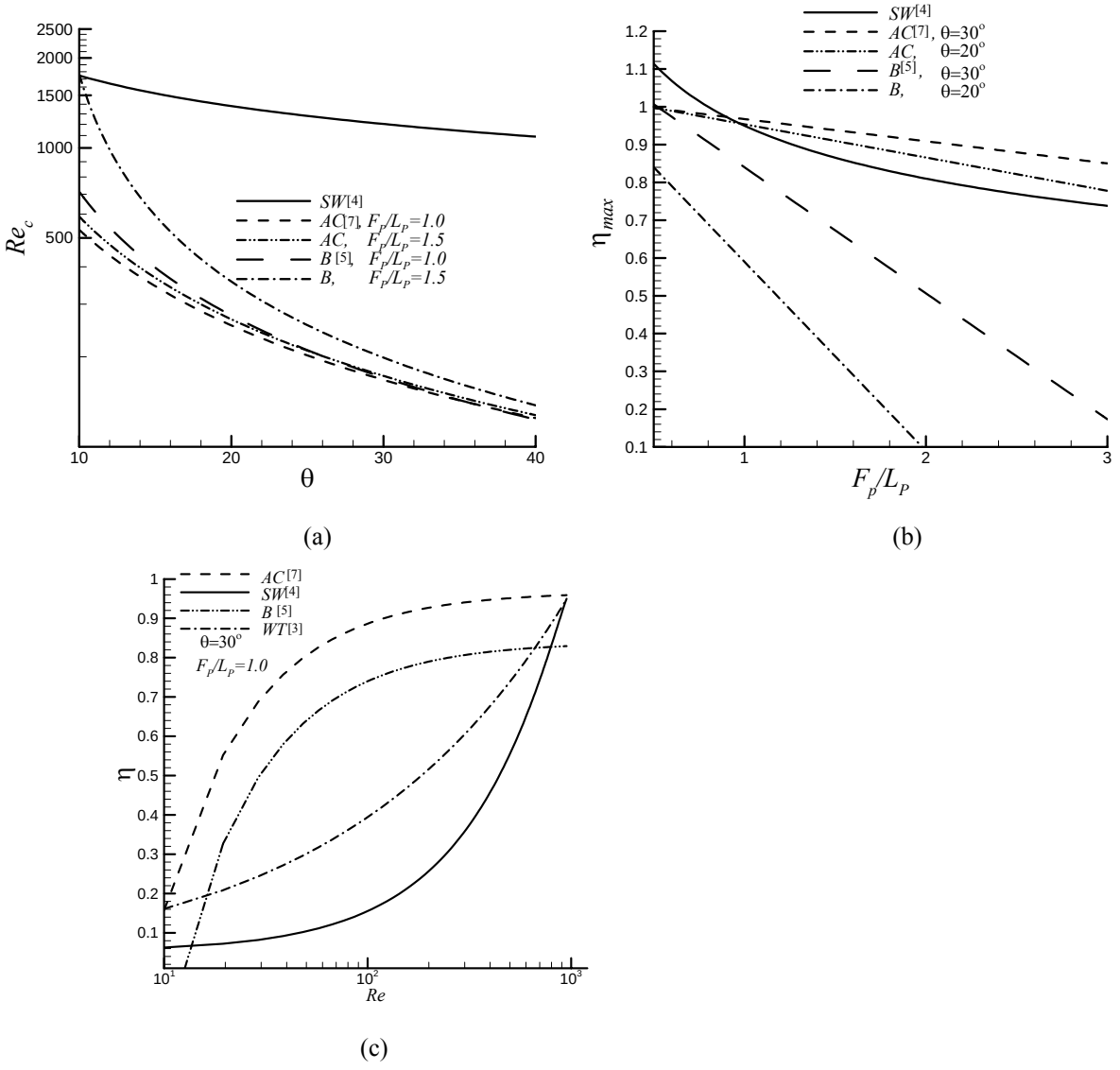

Figure 1.1: Previous correlation results, (a) critical Reynolds number versus louver angle; (b) asymptotic value of flow efficiency versus fin pitch ratio; (c) flow efficiency versus Reynolds number. Note the large qualitative as well as quantitative discrepancies between the correlations.

An important omission in all previous correlations (both numerical and experimental) is the effect of fin thickness ratio. The fin thickness ratios are completely different in these studies. Thickness ratio in AC's numerical calculations is zero, in B's experiments, it varied from 0.089 to 0.106, while in WT's experiments it was fixed at 0.0423.

Our objective in this paper is to use over 200 high resolution numerical simulations done over the past three to four years to develop a broader and consistent relationship between flow efficiency and multilouver geometry and Reynolds number. We study the effect of fin pitch, louver angle, fin thickness, and flow depth on flow efficiency to obtain a mathematical model, which is then used to develop a correlation for flow efficiency.

1.2. Numerical Method and Computational Geometry

The governing equations for momentum and energy conservation are solved in a general boundary conforming coordinate system. They are discretized with a conservative finite-volume formulation. Details about the time-integration algorithm, treatment of boundary and louver surface conditions, and validation of the computer program can be found in Tafti et al. [8]. The base configuration used in these calculations consists of an entrance and exit louver with four louvers on either side of the center or redirection louver. Figure 1.2 shows the base fin geometry and the corresponding computational domain which is resolved by 15 computational blocks, one for each louver, two each for the entrance, exit and redirection louver. The exit domain extends approximately 5.5 non-dimensional units downstream of the exit louver. Periodic boundary conditions are applied in the transverse direction, while Dirichlet boundary conditions are specified at the entrance to the array.

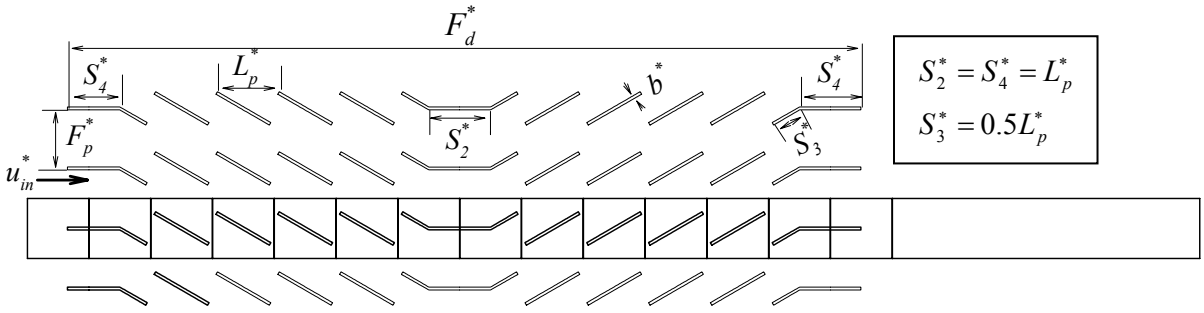

Figure 1.2: Geometrical parameters of louvered fins and multi-block computational domain. The domain is resolved into 15 blocks, one for each louver, two each for the entrance, exit and middle louver. An exit domain (containing no louver), which extends approximately 5.0 non-dimensional units downstream of the array, is added to ensure that the fully developed boundary condition can be applied at the exit.

All results reported in this paper are for a resolution of 96x96 cells per block (total resolution of 138,240 cells). For the unsteady cases, time-averaged values are presented. The average momentum, energy, and mass residues are of the order of $1x10^{-8}$ at each time step.

Table 1.1 summarizes the base geometrical parameters studied in this paper. Two fin pitch ratios (1.0 and 1.5) are studied with variations in louver angle (15, 20, 25, and 30 degrees), and three thickness ratios (0.05, 0.1 and 0.15) are chosen. Reynolds number based on louver pitch is nominally varied from 50 to 1200.

Table 1.1. Summary of non-dimensional geometrical parameters for the basic cases investigated. Nominal Reynolds number range varied from Re_{in} = 50 to 1200.

F_p	θ	b	F_d
1.0	30	0.05	13
		0.1	

		0.15	
	25	0.1	
		0.05	
	20	0.1	
		0.15	
	15	0.1	
	30		17
			13
1.5	25	0.1	
	20		13
	15		

1.3. Validation and Evaluation of the Current Numerical Method

A grid independency study was performed at a resolution of 128x128 cells in each block (a total of 245,760 cells). As shown in Figure 1.3, the time averaged mean flow angles at most of the louvers are identical. Both, non-dimensional heat capacity and Nusselt number calculated on the 96x96 grid are within one percent of the fine grid calculation (not shown).

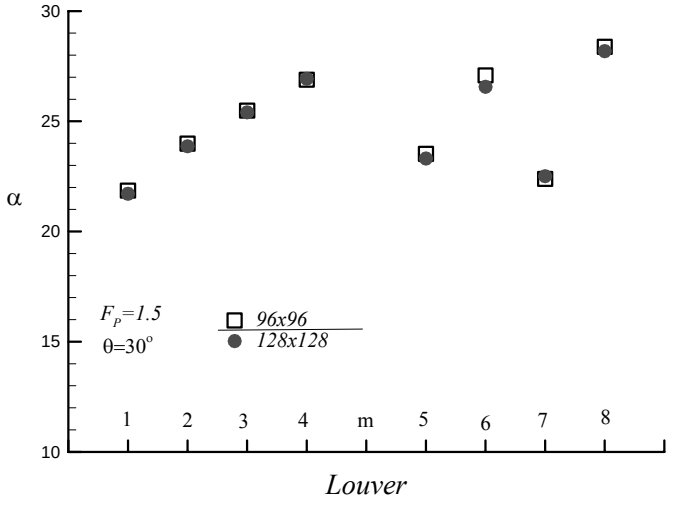

Figure 1.3: A comparison of louver by louver distribution of flow angles at Reynolds number of 1000 for two mesh resolutions per computational block.

To further validate the numerical procedure, we have simulated the multilouvered geometry used in the experiments of DeJong and Jacobi [6]. They performed flow visualization experiments to obtain flow efficiencies together with mass transfer experiments to quantity the heat transfer coefficient. In the experimental setup, the ratio of fin pitch to louver pitch is 1.09, thickness ratio is 0.1, and louver angle is set to 28 degrees, with 7 louvers on either side of the redirection louver. Results from the numerical simulations on an identical geometry are shown in Figure 1.4(a-d). Figure 1.4(a-b), compares the experimental dye path with streamlines injected at the inlet plane of the louver bank (flow is from right to left) at a Reynolds number of 400. The dye, injected between the first and second rows, traverses to the fifth row at the redirection louver. The experimental flow efficiency is[3]:

[3] In DeJong and Jacobi's report, it was 0.77.

$\eta_{\exp} = \frac{N}{D} = \frac{3.5F_P}{9L_P \tan(28^0)} = 0.797$. The streamline pattern obtained from the numerical simulations is nearly identical to the experiments. The average flow angle for the upstream louvers is 22.76 degrees, whereas it is 22.98 degrees for the downstream louvers. The calculated flow efficiency is: $\eta = \frac{\alpha_{mean}}{\theta} = \frac{22.87^0}{28^0} = 0.81$, which agrees very well with the experiments (within 2%).

Figure 1.4 (c) compares the numerical versus experimental flow efficiencies for three Reynolds numbers. In general, the numerical flow efficiencies are predicted slightly higher than the experiments. Figure 1.4(d) plots the experimental and numerical Nusselt numbers. The Sherwood number in DeJong's report for the whole louvered fin is 23.5[4] at the Reynolds number 400, which corresponds to a Nusselt number of 15.76. This compares well with the numerical value of 15.77. Similar good agreement is obtained at Reynolds numbers = 150, 700 and 990.

[4] The Sherwood number in DeJong's experiments for this geometry is only available at Re=270 and 600.

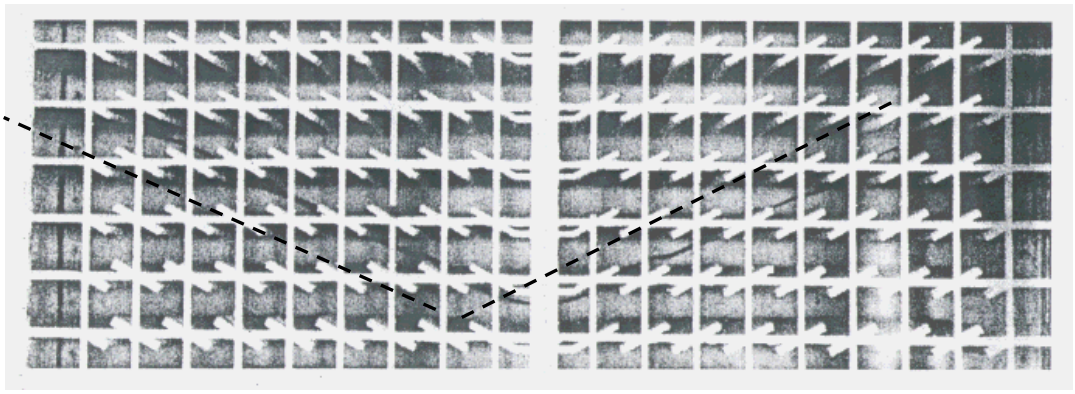

(a)

F_P=1.09, b=0.1, θ=28°

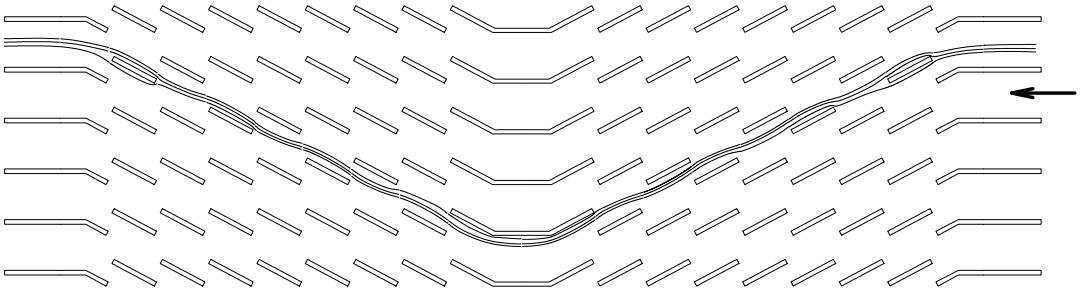

(b)

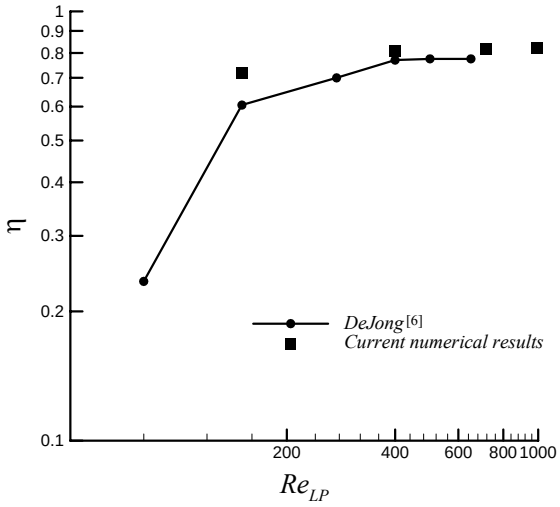

(c)

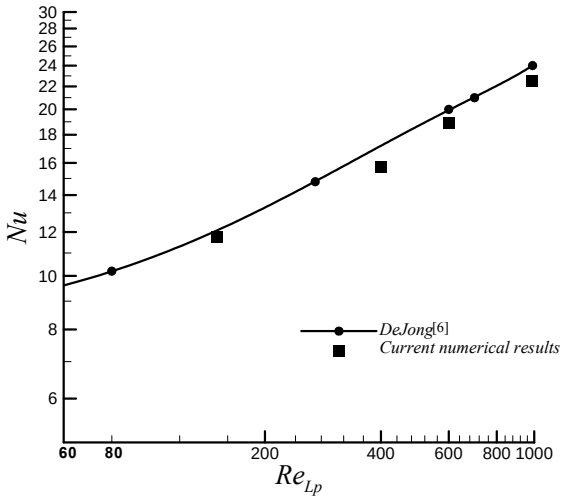

(d)

Figure 1.4: (a-b) Comparison between calculated streamlines from numerical simulations and dye flow trace from experimental tests. Flow is from right side and is nearly parallel to louver direction at the Reynolds number 400; (c) comparison of flow efficiency; (d) the comparison of the Nusselt number.

1.4. Results

1.4.1 Effect of Fin Pitch Ratio and Louver Angle

Figure 1.5 (a) plots flow efficiency versus Reynolds number for different fin pitch ratios and louver angles for developing flow in the louver bank. Results show a strong dependency on both these parameters. Generally, flow efficiency increases with increase in Reynolds number and louver angle, and with decrease in fin pitch ratio. At $\mathrm{Re}_{in} = 50$, flow efficiency increases by 33% after reducing the fin pitch ratio from 1.5 to 1.0 for 30 degree louvered fins, whereas a more than 130% increment is found when louver angle is increased from 15 to 30 degrees for the same fin pitch ratio of 1.0. It is found that the asymptotic value of flow efficiency depends on fin pitch ratio as well as louver angle. For the small fin pitch ratio, $F_P = 1.0$, the asymptotic value varies from 0.75 for 15 degree louvers to 0.94 for 30 degree louvers, whereas smaller variations are present for the larger fin pitch ratio studied. It is observed that the effect of louver angle is stronger for smaller fin pitch ratio. The rate of increment of flow efficiency in the transition region from duct to louver directed flow decreases rapidly with increase of Reynolds number, which is consistent with the results of AC and B, and contrary to the results of SW where nearly a constant rate of increase was found.

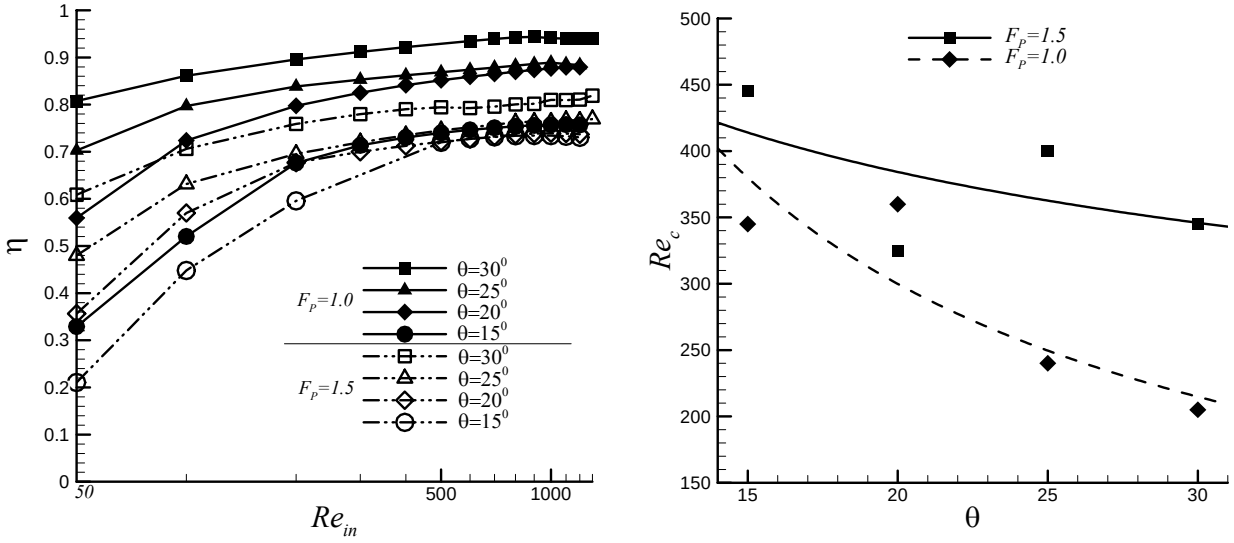

(a) (b)

Figure 1.5: (a) Flow efficiency versus Reynolds number with different fin pitch ratios and louver angles; (b) critical Reynolds number (at which the flow efficiency reaches 95% of the asymptotic value) versus louver angle for two fin pitch ratios.

Figure 1.5 (b) plots the critical Reynolds number versus louver angle. Critical Reynolds number is based on the Reynolds number at which the flow efficiency reaches 95% of the maximum flow efficiency. The critical Reynolds number decreases with increase in louver angle, and decrease in fin pitch. Hence at low Reynolds number, small fin pitch ratio and large louver angles are favorable for high flow efficiency. This trend is consistent with previous correlations of AC and B. For a fin pitch ratio of 1.0 and 15 degree louvered fins, the critical Reynolds number in the current study is around 350, which agrees well with 360 in AC and B's results, whereas in SW's results the critical Reynolds number is almost as high as 1500.

1.4.2 Effect of Thickness Ratio and Flow Depth

In previous experimental and numerical work, the effect of fin thickness on flow efficiency has not been studied, nor has it been included in correlations of flow efficiency. Figure 1.6 (a) plots the flow efficiencies with three different thickness ratios (0.05, 0.1, 0.15) at two louver angles, 20 and 30 degrees. The results show the clear dependency on thickness ratio: thicker louvers lower flow efficiency for both louver angles; the deterioration of flow efficiency with thickness is more severe at small louver angles. At low Reynolds number ($\mathrm{Re}_{in} = 50$), more than a 55% increment is found on reducing the thickness from 0.15 to 0.05 in 20 degree louvered fins, whereas only a 13% increment is found in the 30 degree geometry.

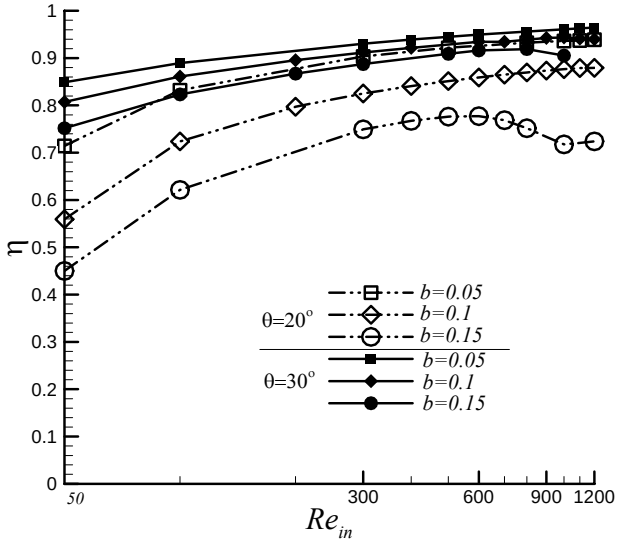

(a)

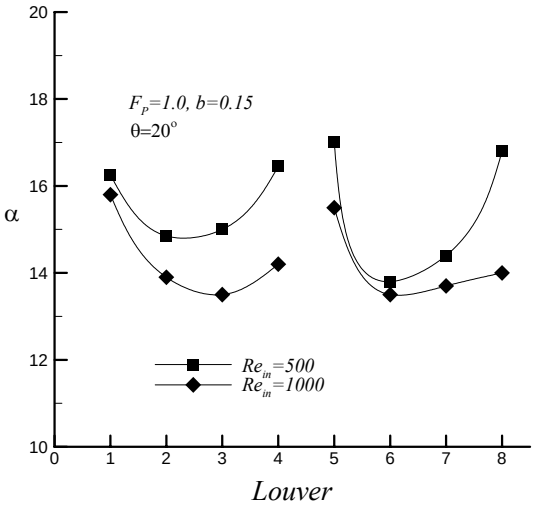

(b)

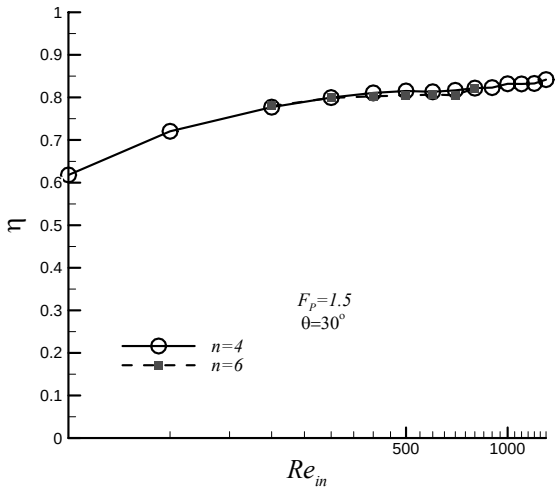

(c)

Figure 1.6: (a) Flow efficiency versus Reynolds number for different thickness ratios and louver angles; (b) flow angles at two Reynolds numbers, 500 and 1000; (c) effect of flow depth on flow efficiency (*n* denotes number of louvers on either side of redirection louver).

It is observed that for thicker fins (b=0.15), a drop in flow efficiency is incurred as the Reynolds number increases beyond a certain value, followed by a recovery. At small louver angles the drop in flow efficiency occurs earlier than with large louver angles. As louver thickness increases, the open flow area between adjacent louvers is reduced. The percentage reduction in the flow area is larger for smaller louver angles. As Reynolds number increases, thicker louvers are more prone to develop large recirculation zones on the louver surface. The recirculation zones further block the flow path between louvers, hence decreasing the flow efficiency. As the Reynolds number increases further, the separated shear layer becomes unstable, with subsequent vortex shedding. This partially frees up the flow passage between louvers, and lets the flow efficiency recover to a higher value. This is seen in the distribution of flow angles at individual louvers in Figure 1.6 (b). The flow angles are higher at Re_{in} = 500, than at 1000 when recirculation zones dominate the flow field around louvers.

The effect of flow depth on flow efficiency was investigated by performing additional numerical calculations for the louvered fins with two more louvers on either side of the redirection louver for a 1.5 fin pitch ratio, 30 degree louver angle and 0.1 thickness ratio. The increase in flow depth has very little effect on flow efficiency, as shown in Figure 1.6 (c). For Reynolds number less than 300, two more calculations were also made for louvered fins with a 1.41 fin pitch ratio, 20 degree louver angle, and 0.15 fin thickness ratio. One configuration had 12 louvers (6 louvers on either side of redirection louver) and the other 14. At Reynolds number 50, flow efficiency for the two was identical.

1.4.3 Model for Predicting Trends in Flow Efficiency

The accurate prediction of flow efficiency requires that all geometrical and nonlinear hydrodynamic effects be taken into account. In this section we develop a simple model for predicting flow efficiency based solely on geometrical information and its first-order effect on the hydrodynamics. Using this model and the database of calculated flow efficiencies, we then develop a general correlation for flow efficiency in the next section.

For a given fin geometry and Reynolds number, air flow through the louver bank follows the path of least resistance. The incoming flow can be decomposed into two fluid streams: one that flows between two fins or duct directed flow, and the other which flows in the louver direction as shown in Figure 1.7 (a). If U_F is the bulk flow velocity in the direction parallel to the fin, and U_L, the bulk velocity parallel to the louver direction, then using the decomposition in Figure 1.7 (b), the following relationship is satisfied:

$$\tan\alpha = \left(\frac{U_L \sin\theta}{U_F + U_L \cos\theta}\right). \tag{6}$$

In the small to medium angle limit, Eqn.(6) can be simplified to obtain an expression for flow efficiency as:

$$\eta = \frac{\alpha}{\theta} = \left(\frac{U_L}{U_F + U_L}\right) = \frac{r}{1+r}, \text{ where } r = \frac{U_L}{U_F}. \tag{7}$$

Equating the pressure loss for the two fluid streams in a parallel flow circuit, the following equation is satisfied:

$$\frac{f_F F_{d,F} U_F^2}{D_{h,F}} = \frac{f_L F_{d,L} U_L^2}{D_{h,L}}. \tag{8}$$

Here, f, F_d, D_h is the friction factor, flow depth, and hydraulic diameter, respectively. To first order, the hydraulic diameter of the two flow paths can be approximated by the channel widths between fins (d_F) and that between louvers (d_L), as shown in Figure 1.7 (b), and the flow depth ratio as $F_{d,F} / F_{d,L} = \cos\theta$. Both friction factors can be assumed proportional to a negative power of Reynolds number, $f = c / \mathrm{Re}^e$. Assuming that the constant *c,* and exponent *e* are equal for the two fluid streams, the ratio $f_F / f_L = \left(U_L d_L / U_F d_F\right)^e$. Hence, from eqn. (8), $U_L / U_F = r = (d_L / d_F)^{(1+e)/(2-e)} \cos^{1/(2-e)} \theta$. Substituting in eqn. (7), an expression for flow efficiency follows as:

$$\eta \propto \frac{d^{(1+e)/(2-e)}}{\cos^{1/(e-2)} \theta + d^{(1+e)/(2-e)}}, \tag{9}$$

where $d = \dfrac{d_L}{d_F} = \dfrac{\sin(\theta) - b}{F_P - \sin(\theta) - b\cos(\theta)}$ is the characteristic *flow efficiency length scale ratio*.

The above formulation reveals the relationship between the flow efficiency and fin pitch ratio, thickness ratio, and louver angle. As the ratio $d \to 0, \eta \to 0$; conversely as $d \to \infty, \eta \to 1.$ In reality though, for typical louver geometries, $0 < d < 1$. Eqn. (9) relates the trends in flow efficiency to geometrical parameters, and it can be shown from eqn. (9) that $\eta \propto d$, i.e, η is a monotonic function of *d*.

The individual effect of the three geometrical parameters, fin pitch ratio, thickness ratio and louver angle on flow efficiency can be studied by evaluating their effect on the ratio *d*. The derivatives of function *d* with respect to the three variables are written as:

$$d'_F = \frac{-1}{(F - \sin(\theta) - b\cos(\theta))^2},$$

$$d'_\theta = \frac{F\cos(\theta) - b - b\cos(\theta) + b\sin^2(\theta)}{(F - \sin(\theta) - b\cos(\theta))^2},$$

$$d'_b = \frac{-F + \sin(\theta) + b\cos(\theta) + \sin^2(\theta) - b\sin(\theta)}{(F - \sin(\theta) - b\cos(\theta))^2}.$$

To verify the relevance and importance of ratio *d*, we compare predicted trends in flow efficiency with known results and also validate some unexpected trends predicted by *d*. It can be seen that d'_F is always less than zero, so that increasing fin pitch ratio always has a negative effect on flow efficiency. Increasing louver angle has a positive effect on flow efficiency almost in all parameter ranges, except under some very unusual conditions, such as fin pitch ratio less than 1.0, louver angle larger than 70 degrees and thickness ratio larger than 0.4 to satisfy the inequality $F\cos(\theta) - b - b\cos(\theta) + b^2\sin(\theta) < 0$. Increasing thickness ratio has a negative effect on flow efficiency for large fin pitch ratios, and small louver angle. Conversely, for small fin pitch ratio (less than 1.0), and large louver angles (larger than 40 degrees), increasing thickness, increases the flow efficiency.

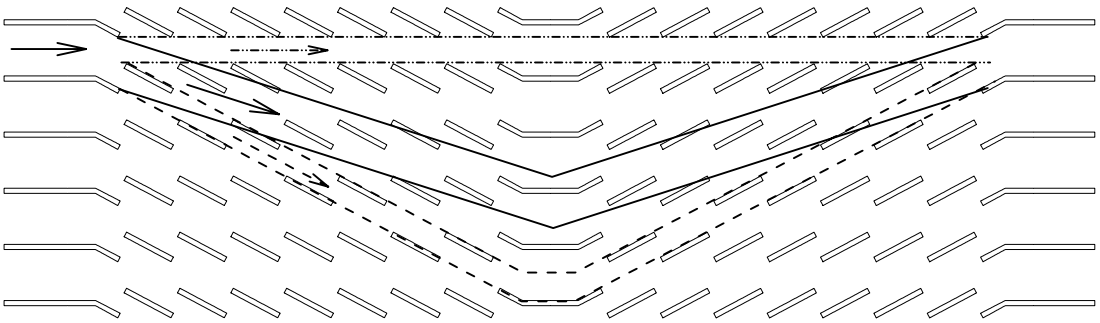

(a)

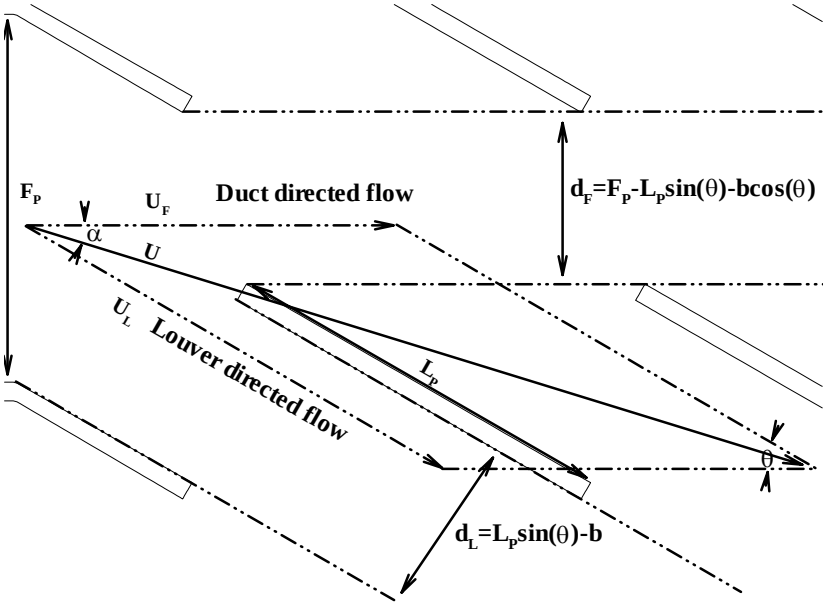

(b)

Figure 1.7: Schematic plot of flow in multi-louvered fins. The channel bounded with solid lines represents the actual flow path, the channel with dash lines represents ideal louver directed flow, whereas dash-dot channel represents duct directed flow. In the analytical model, the actual flow passage is decomposed into the two ideal flow passages: duct directed and louver directed channels.

Figure 1.8 (a) shows iso-surfaces of *d* at *d*=0.32, 0.74 and 1.55. Generally, high values of *d* (and flow efficiency) are located in regions of large louver angles and small fin pitch ratios. Conversely, low values of *d* exist in regions of small louver angles and large fin pitches. Hence, the trends in *d* indicate that large louver angles can compensate for the loss in flow efficiency brought about by large fin pitches.

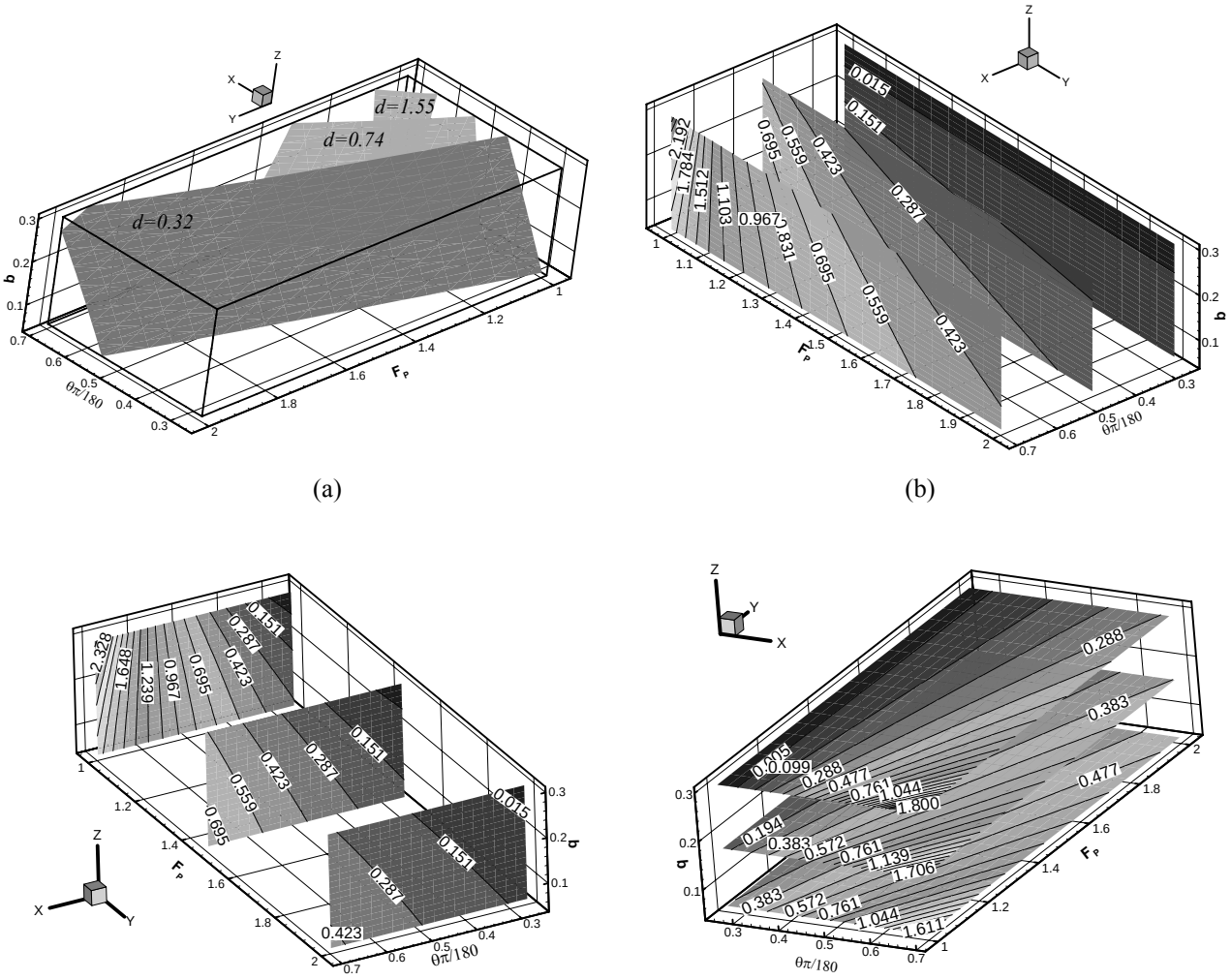

Figure 1.8: Predicted trends from model. High values of *d* indicate high flow efficiency: (a) combined effect of three parameters on flow efficiency at three levels, *d*=0.32, 0.74 and 1.55; (b) effect of fin pitch ratio and thickness ratio at three louver angles; (c) effect of louver angle and thickness ratio at three fin pitch ratios; (d) effect of fin pitch ratio and louver angle at three thickness ratios.

Figure 1.8 (b) shows contours of *d* at three louver angles, 10, 30 and 40 degrees. At a louver angle of 10 degrees, ratio *d* is very small. Both fin pitch and thickness ratios have a very slight effect on *d*, and *d* decreases slightly as fin pitch and thickness ratio increase. At a louver angle of 30 degrees, the effect of fin pitch and thickness ratio becomes more apparent. As louver angle increases to 40 degrees, fin pitch has a significant effect on *d*. We note that the thickness ratio has two completely opposite effects at small and larger fin pitch ratios. For fin pitch ratios less than 1.1, *d* (flow efficiency) increases with increase of thickness ratio; at $F_P = 1.1$, *d* is not affected by thickness ratio; and for $F_P > 1.1$, *d* decreases with an increase in thickness ratio.

Figure 1.8 (c) plots the effect of louver angle and thickness ratio on *d* for three fin pitch ratios, 1.0, 1.5 and 2.0. It is found that louver angle has a strong effect on *d* at small fin pitch ratios, whereas the sensitivity of *d* to louver angle decreases as fin pitch increases. However, larger louver angles do compensate for high fin pitches by

increasing *d*. We again note the trend reversal of the effect of thickness on *d* at large louver angles and small fin pitches. The normal trend, which is present for moderate to high fin pitches, and moderate to low louver angles, is a decrease in *d* and flow efficiency with an increase in thickness. The trend reversal can be seen clearly in Figure 1.8 (b-c) at $F_P = 1.0$, when the slope of constant *d*-lines change at around 40 degree louver angle. Although, counter-intuitive, the result is reasonable because for large louver angles, the percentage reduction of the fin gap caused by an increase in thickness ratio is smaller than the corresponding reduction of the gap between two louvers. This leads to conditions more favorable to louver directed flow. However large louver angles and thick louvers are prone to develop large recirculation zones on louvers at relatively low Reynolds numbers, which lowers the effective *d*, and subsequently the flow efficiency.

Finally, Figure 1.8 (d) plots the effect of louver angle and fin pitch ratio on *d* on planes of constant thickness. Consistent with previous results, flow efficiency (proportional to *d*) is higher for larger louver angles and smaller fin pitch ratios. The effect of fin pitch ratio and louver angle is more significant at larger fin thickness.

1.4.4 General Correlation for Flow Efficiency

In the previous section, a first order relationship between flow efficiency and geometrical parameters was introduced in eqn. (9). In this section, eqn. (9) is used as the foundation for developing a general correlation for flow efficiency. We first use eqn. (9) to set the value of flow efficiency based solely on trends predicted by geometrical information (given by η_1). This establishes the correct base trends in flow efficiency, and further corrections are added to match the absolute values. In the next step, an additive factor (given by η_2) is introduced to match the asymptotic value of flow efficiency for a given geometry. Finally, η_3 adjusts the asymptotic value by introducing a Reynolds number dependency. All, $\eta_{1\text{-}3}$ are functions of the louver geometry, whereas, only η_3 has a Reynolds number dependence in it.

To obtain a reasonable value of the exponent *e* in eqn. (9), predicted trends with different values of *e* are compared to trends in asymptotic values of flow efficiency for different geometries (or different values of *d*). These are plotted in Figure 1.9. It is found that $e \to 0$ gives the best representation of the trends seen in the asymptotic flow efficiencies. It is worth noting, that the exponent $e \to 0$, represents the limiting case for fully rough channels in which there is no or very little Reynolds number dependence of friction factor. Hence, the final form of the correlation is given by:

$$\eta = \eta_1 + \eta_2 + \eta_3 \tag{10}$$

where,

$$\eta_1 = \frac{d^{1/2}}{d^{1/2} + 1/\cos^{1/2}(\theta)},$$

$$\eta_2 = \frac{0.357}{(F_P b)^{0.1}} \left(\frac{30}{\theta}\right)^{(F_P - 0.9)},$$

and $$\eta_3 = -\frac{70b}{\mathrm{Re}_{in}^{(0.38/F_P^{1.1} + 0.02\theta)}},$$

where $d = \dfrac{d_L}{d_F} = \dfrac{\sin(\theta) - b}{F_P - \sin(\theta) - b\cos(\theta)}$,

in the range

$$0.794 < F_P < 2.0;$$
$$15^\circ < \theta < 50^\circ$$
$$0.05 < b < 0.2;$$
$$50 < \mathrm{Re}_{in} < 1200$$
$$0.1 < d < 1.9.$$

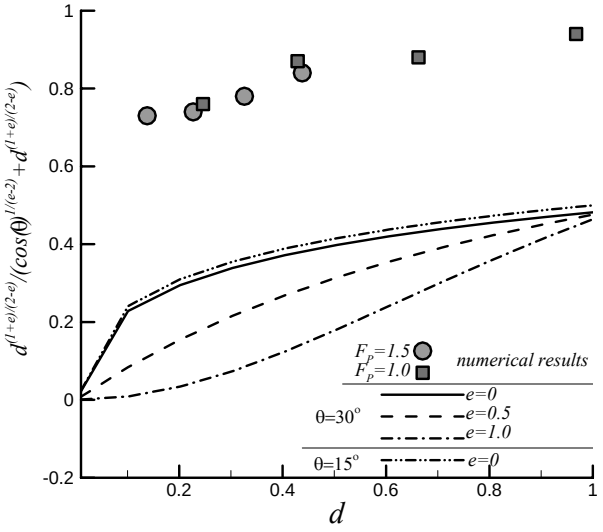

Figure 1.9: Comparison of the trends in asymptotic flow efficiency from numerical simulations with predicted model trends for different values of d. The exponent, $e = 0$ shows the best agreement.

Figure 1.10 shows the comparison of flow efficiencies obtained from the above correlation and numerical calculations on which the correlation is based (cases in Table 1.1). The errors in the correlation are larger at low Reynolds numbers, small louver angles, and large fin pitches.

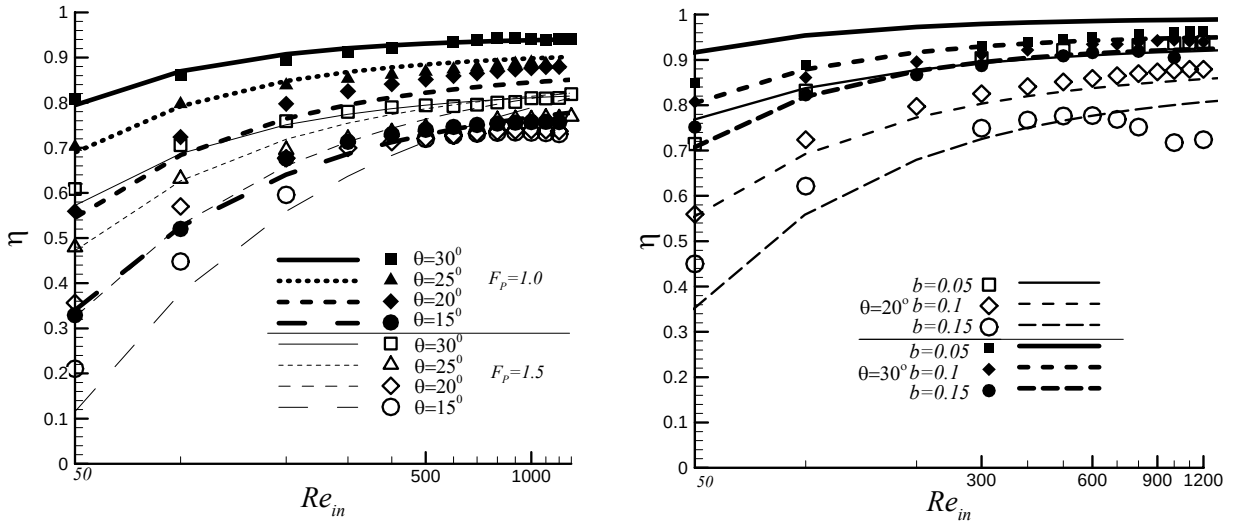

(a) (b)

Figure 1.10: Comparison of flow efficiencies obtained by eqn. (10) and numerical results. (a) geometries with different louver angles and fin pitch ratios at a thickness ratio of 0.1; (b) geometries with different thickness ratio at fin pitch 1.0 and louver angles 20 and 30 degrees.

We further test the accuracy of the correlation by using it to predict flow efficiencies in louver configurations not used to construct the correlation. This is shown in Figure 1.11. In these cases, fin pitch ratios vary from 0.794 to 2.0, louver angle from 20 to 40 degrees, with different thickness ratios. The number of louvers, geometry of inlet, exit, and redirection louvers are also different from the geometries used to construct the correlation. The correlation predicts the flow efficiency with good accuracy. Additional comparisons are presented for extreme conditions of high louver angles and thick louvers. One set is for louvered fins with large louver angles (40, 50 and 60 degrees) at two fin pitch ratios, 1.5 and 2.0, with a thickness ratio of 0.1, the other is for fins with two thickness ratios (0.1 and 0.2) at a large louver angle (40 degrees) and a fin pitch ratio of 1.0. The complete geometrical parameters are described in Table 1.2. Figure 1.11(c-d) plots the predicted flow efficiency versus the numerical calculations. Even for the extreme louver geometries, the correlation shows a high degree of accuracy in predicting the numerical data, up to θ=50 degrees. The correlation does not predict the drop in flow efficiency for θ>50 degrees, which is a result of blockages between louver passages caused by massive flow separation. Figure 1.11 (d) tests the prediction capability of the correlation at large thickness ratios. For small fin pitch, and high louver angle, the ratio d predicts an increasing trend in flow efficiency with thickness. This is countered by recirculation zones which are more prevalent for thick louvers. Both these effects combine to give a near constant flow efficiency.

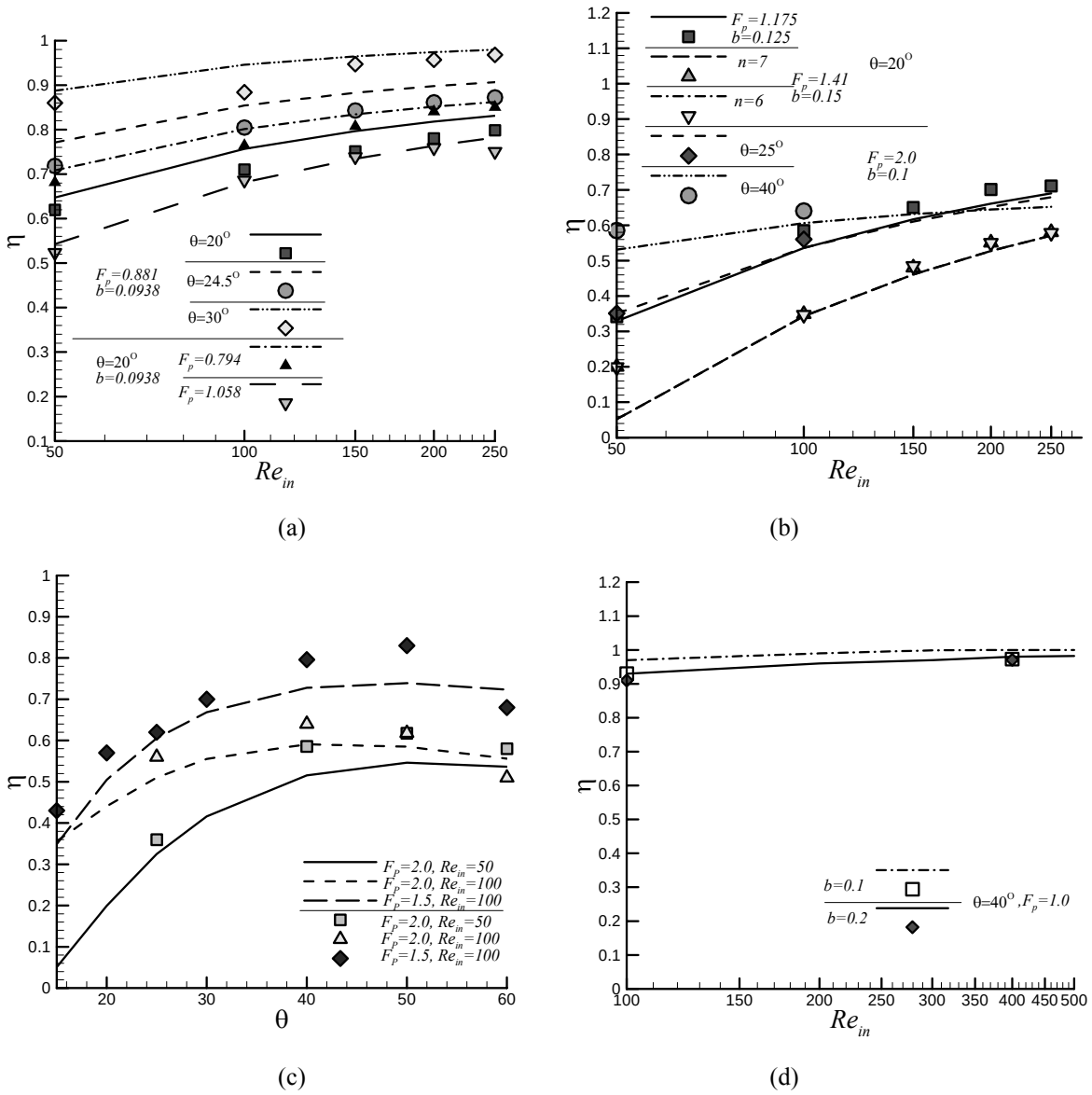

Figure 1.11: Comparison of flow efficiency obtained from eqn. (10) with numerical calculations over a large range of fin pitch ratio (from 0.794 to 2.0) at different louver angles (from 20 to 60 degrees) and thickness ratios (0.1 to 0.2). These data points were not used to construct the correlation.

Table 1.2. Summary of calculations at low Reynolds numbers with large louver angles and thickness ratios.

F_p	b	θ	Re	F_d
1.5	0.1	25	50	13
		30		
		40		
		50		
		60		
2.0		25	50	

		40	100	
		50		
		60		
1.0	0.1	40	100	
	0.2		400	

A comparison between the current and previous correlations is plotted in Figure 1.12, for F_p = 1.0 and 1.5, louver angle 30 degrees, and thickness ratio of 0.1. For F_p = 1.0, current results agree well with AC, whereas large differences are observed at F_p = 1.5 because of the fully-developed assumptions. B's correlation gave the lowest values for both fin pitch ratios. The trends exhibited by SW's correlation are opposite to the other correlations.

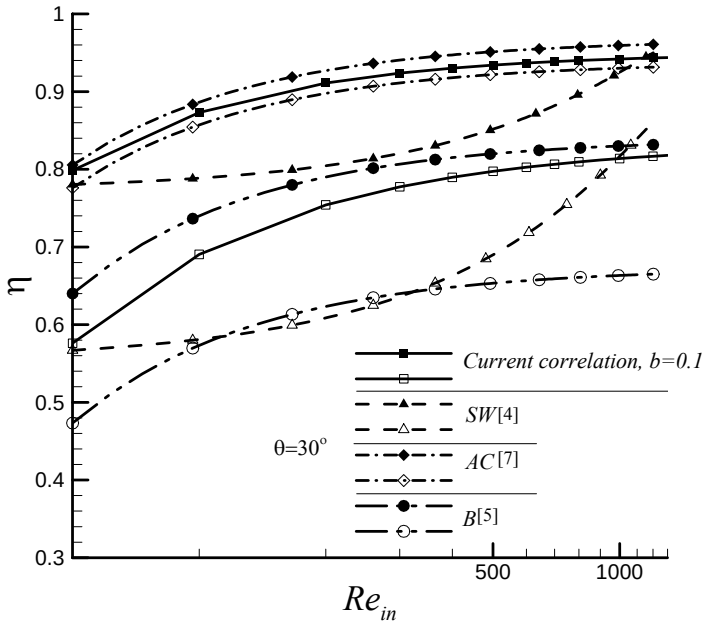

Figure 1.12: Comparison of flow efficiency predicted by eqn. (10) and previous correlations.

Finally, Figure 1.13 (a) and (b) plot the prediction error of the current correlation. Results show that more than 95% of the calculation results are represented by the correlation within 10% error, with 80% of calculation results represented within 5%. The larger error at the Reynolds number of 100 in Figure 1.13(b) is caused by the inclusion of the cases with large louver angles (50 and 60 degrees).

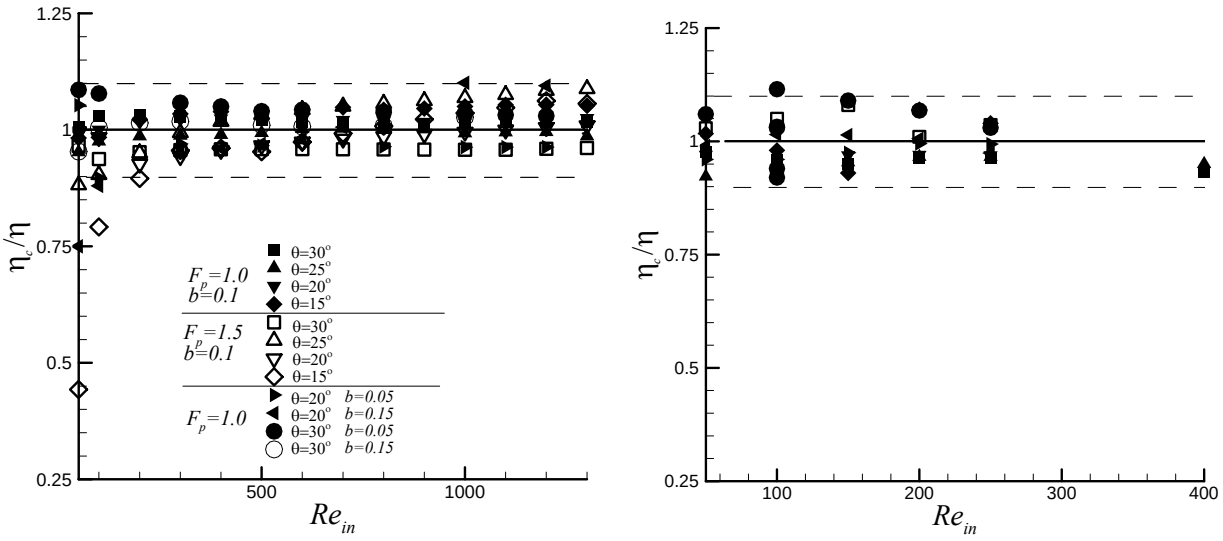

(a) (b)

Figure 1.13: Ratio of flow efficiency predicted by eqn. (10) to calculated flow efficiencies. Error within ±10% is bounded by dashed lines; (a) for the basic cases on which the correlation was based; (b) for all the other cases.

1.5. Conclusions

Flow efficiency has a strong effect on the heat transfer capacity in multilouvered fins. A review of past correlations has shown considerable differences in their ability to predict flow efficiency consistently and accurately. The present paper presents a general correlation for flow efficiency with the aid of a large database of high fidelity numerical simulations. Results show that flow efficiency is strongly dependent on geometrical parameters, especially at low Reynolds numbers. Flow efficiency increases with Reynolds number and louver angle, while decreasing with fin pitch and thickness ratio. Compared to fin pitch, louver angle has a stronger effect. Louver thickness effect on flow efficiency is also significant for small louver angles. A relationship for the trend in flow efficiency is developed based on geometrical and first-order hydrodynamic effects. The relationship is then supplemented by numerical results to develop a general correlation for flow efficiency with a geometrical dependence on fin pitch, louver thickness ratio, and louver angle. Comparisons show that the correlation represents more than 95% of numerical predictions within a 10% error band, and 80% of predictions within a 5% error band over a wide range of geometrical and hydrodynamic conditions.

1.6. References

1. F. N. Beauvais, An Aerodynamic Look at Automobile radiators, SAE paper No. 650470, 1965.
2. C. J. Davenport, Heat Transfer and Fluid Flow in Louvered Triangular Ducts, Ph.D. Thesis. CNAA, Lanchester Polytechnic, 1980.
3. R. L. Webb and P. Trauger, Flow structure in the louvered fin heat exchanger geometry, Experimental Thermal and Fluid Science, Vol. 4, pp. 205-217, 1991.
4. A. Sahnoun and R. L. Webb, Prediction of Heat Transfer and Friction for the Louver Fin Geometry, Journal of Heat Transfer, Vol. 114,:893-900, 1992.

5. K. D. Bellows, Flow Visualization of Louvered-Fin Heat Exchangers, Masters Thesis, University of Illinois at Urbana-Champaign, 1996.

6. N. C. DeJong and A. M. Jacobi, Flow, Heat Transfer, and Pressure Drop Interactions in Louvered-Fin Arrays, ACRC TR-146, University of Illinois at Urbana-Champaign, January 1999.

7. A. Achaichia and T. A. Cowell, Heat Transfer and Pressure Drop Characteristics of Flat Tube and Louvered Plate Fin Surfaces, Experimental Thermal and Fluid Science, 1988, 1:147-157.

8. D. K. Tafti, L. W. Zhang and G. Wang, Time-Dependent Calculation Procedure for Fully Developed and Developing Flow and Heat Transfer in Louvered Fin Geometries, Num. Heat Transfer, Part A, 35:225-249, 1999.

Chapter 2. Effect of Louver Angle on Performance

Abstract

The paper studies the effect of large louver angles on the performance of large pitch multilouvered fins at low Reynolds numbers. The Reynolds number based on face velocity and louver pitch is varied between 50 and 300. Louver angles are varied from 20° to 60° for fin pitch ratios of 1.5 and 2.0. It is found that increasing louver angle has a favorable effect on flow efficiency up to a certain point, beyond which the flow efficiency decreases. The maximum flow efficiency is realized at smaller louver angles as the Reynolds number increases. The drop in flow efficiency is attributed to the development of recirculation zones which act as blockages. In spite of the decrease in flow efficiency, the heat transfer coefficient increases with louver angle for all the cases studied. It is found that as louver angle increases, impingement heat transfer at the leading surface of louvers becomes a dominant mode of heat transfer. Friction factors also increase with louver angle, primarily due to an increase in form drag.

Nomenclature

$\overrightarrow{a^j}$	contravariant basis vectors
b	fin thickness,
F_p	non-dimensional fin pitch,
F_d	non-dimensional flow depth,
$\sqrt{g}$	Jacobian of transformation
g^{jk}	contravariant metric tensor
k	thermal conductivity,
L_p^*	dimensional louver pitch (characteristic length scale),
Nu^1	non-dimensional heat flux,
Nu^2	non-dimensional heat transfer coefficient,
Pr	Prandtl number,
q	non-dimensional heat flux,
Re_{in},Re	Reynolds number,
T	temperature,
u_i	Cartesian velocity vector
U^j	Contravariant velocity components
$S_{1,2,3}$	Dimensions of inlet, redirection and exit louver; S_1=S_2=1, S_3=0.5.

Greek symbols

□	flow angle,
η	flow efficiency,
ν	kinematic viscosity,
θ	louver angle.

Superscripts

*	dimensional quantities.

Subscripts

f, fin	based on fin.

2.1 Introduction

Multi-louvered fin compact heat exchangers are used extensively in the automobile, heating, ventilation and air-conditioning industries. A typical flat-tube louvered heat exchanger with rectangular channels is shown in Figure 2.1(a). Three important factors affect the heat transfer capacity in multi-louvered geometries; they are (a) the dominant flow direction [1, 2], or flow efficiency, (b) the presence of flow unsteadiness and associated large-scale structures [3], and (c) thermal wake interference [4].

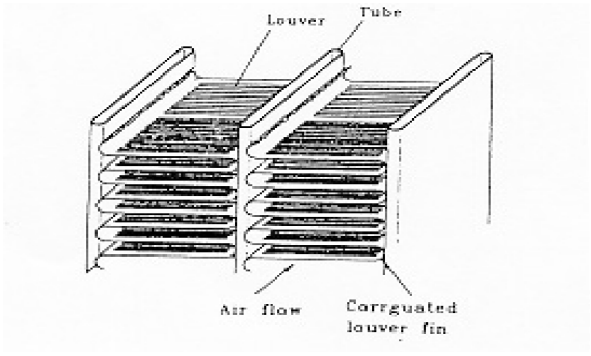

(a)

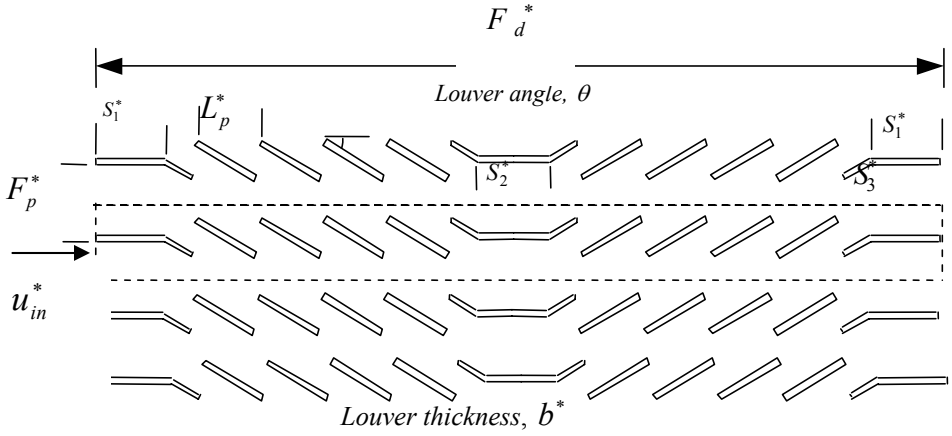

(b)

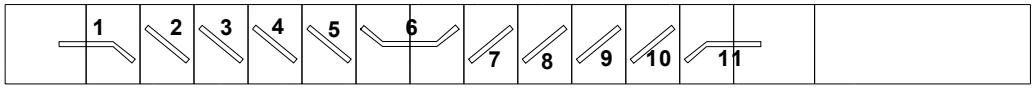

(c)

Figure 2.1: (a) Flat tube louvered heat exchanger; (b) Cross-section of multi-louvered fin array. Dotted lines show the basic computational unit; (c) Multi-block domain decomposition.

Louvers have been extensively studied in the last two decades. Davenport [1] identified that at low Reynolds number there was a flattening of the *j*-factor curve, which he attributed to the transition to duct directed flow. Achaichia and Cowell [5] numerically studied an infinite array of zero thickness louvers and derived an expression for flow angle from their results. In a related study, Achaichia and Cowell [6] reported heat transfer and friction data for 23 sample geometries. Antoniou et al. [7] made turbulent measurements in a louvered fin.

Subsequently Webb and his group [2,8,9] also investigated louvered fins. They developed correlations for flow efficiency based on their data and found that it did not agree with the correlations of Achaichia and Cowell [5]. Springer and Thole [10] found that larger fin pitches resulted in lower average flow angles in the louver passages and longer development lengths.

Several computational studies of multi-louver geometries have been attempted since the 1980s. Various simplifying assumptions made in earlier studies have prevented the use of computations for complete and reliable predictions of multi-louvered fins. These studies assumed louvers of zero thickness and/or fully-developed flow conditions [5], and/or Cartesian grids with a staircase louver surface [11]. The late 80s and early 90s saw considerable progress in the Japanese automotive industry in simulating multi-louvered geometries. Suga et al. [12] and Suga and Aoki [13] used considerable sophistication in their formulation on overlaid grids for representative multi-louvered fins. The overlaid grids allowed the use of orthogonal grids aligned with the louvers, however, interpolations had to be performed at grid junctions. On the other hand, Hiramatsu at al. [14] used oblique or body-fitted grids in the calculation domain. Achaichia et al. [15] studied the flow pattern in multi-louvered fins with the commercial code PHOENICS along with the k-ε turbulence model for high Reynolds numbers.

Bellows [16] experimentally determined the flow efficiency and compared with previously determined flow efficiencies of Achaichia and Cowell [5] and Webb and Trauger [2]. They found that louver angle had a larger effect on flow efficiency than fin pitch ratio. DeJong and Jacobi [17] performed an experimental investigation on pressure drop and heat transfer. Tafti et. al. [3, 4, 18-19] have modeling of air-side heat transfer by applying time-dependent calculations to two-dimensional multi-louvered geometries. Two fin pitch to louver pitch ratios and four louver angles were studied, in addition to the effect of fin thickness. Cui and Tafti [20] and Tafti and Cui [21,22] extended the numerical modeling to three-dimensional aspects of the louver geometry near the louver-tube junction.

Although multi-louvered fins have been studied extensively in the past two decades, scant attention has been given to the low Reynolds number flow regime, partly because of the increased experimental uncertainties experienced in measuring pressure drops and heat transfer. In most applications of multi-louvered heat exchangers the operating Reynolds number seldom increases beyond 500 based on the face velocity and louver pitch. In this range of Reynolds numbers, heat transfer capacity is quite dependent on the direction of flow or flow efficiency. In this respect, small fin pitch ratios ($F_p \leq 1.0$) are advantageous because they force more fluid to flow through the louvers. However, in condenser applications, small fin pitches are prone to water blockages which can substantially reduce performance. Large fin pitches, on the other hand have lower flow efficiencies but are less prone to blockages.

In this paper, the effect of louver angle on flow efficiency and heat transfer coefficient is studied for large fin pitches in the low Reynolds number regime ($\mathrm{Re} \leq 500$). Two fin pitches, $F_p = 1.5$ and 2.0 are studied for louver angles ranging from 20 to 60 degrees.

2.2 Computational Details

The governing equations for momentum and energy conservation in generalized coordinates are discretized with a conservative finite-volume formulation. Both, convection and viscous terms are approximated by second-

order central-difference schemes in a non-staggered arrangement[5]. The computational unit, shown in Figure 2.1 (b) by the dotted lines, consists of one entire row of the louvered fin geometry allowing the inclusion of entrance and exit effects in the flow direction. Periodic boundary conditions are applied in the transverse direction while Dirichlet boundary conditions are specified at the entrance to the louver bank. The application of periodicity simulates a bank of louvers in the transverse direction.

The governing equations are non-dimensionalized by a characteristic length given by the louver pitch L_p^*, a characteristic velocity scale given by the inlet velocity to the array (u_{in}^*) and a temperature scale given by ($T_f^* - T_{in}^*$), where T_f^* is the specified fin surface temperature. The non-dimensionalization results in a characteristic Reynolds number $\mathrm{Re} = \mathrm{Re}_{in} = u_{in}^* L_p^* / \nu$, with Dirichlet boundary conditions $u_{in} = 1, T_{in} = 0$ at the entrance to the computational domain. The Prandtl number is fixed at 0.7 for air. At the fin surface, no slip and no penetration boundary conditions for the velocity field, and $T_f = 1$ for the temperature field are applied. Due to the recovering nature of the flow at the array exit, convective outflow boundary conditions are applied at this boundary. Details about the time-integration algorithm, treatment of boundary and louver surface conditions, and validation of the computer program can be found in Tafti et al. [18].

The configuration used in these calculations consists of an entrance and exit louver with four louvers on either side of the center or redirection louver. For all the calculations in this paper the louver thickness is fixed at b = 0.1. For the entrance and exit louvers, S_1 = 1, and for the center redirection louver, S_2 = 1. Figure 2.1(c) shows the computational domain which is resolved by 15 blocks, one for each louver, two each for the entrance, exit and redirection louver. The exit domain extends approximately 5.5 non-dimensional units (or 55 fin thicknesses) downstream of the array. Each block is resolved by 96x96 finite-volume cells (a total of 138,240 cells). For the unsteady cases, time-averaged values are presented. The resolution used has been shown to be grid independent in earlier studies at Re=1000 [3,4], in which the time-averaged heat transfer coefficient was found to be within 1-2% of that on a 128x128 grid per block. The same resolution has been found to compare very well with experimental data in [23]. It is expected that this resolution is adequate to provide an accurate representation of the flow physics and heat transfer of the low Reynolds number calculations presented in this paper.

2.3 Characterization of Flow Efficiency, Friction, and Heat Transfer

Flow efficiency (η) is used to describe the percentage of the fluid flowing along the louver direction. A 100% efficiency represents ideal louver directed flow while 0% represents complete duct directed flow. Duct directed flow refers to the flow in the louver bank primarily aligned with the stream-wise direction, while louver directed flow mainly passes through the louvers. Duct directed flow has a detrimental effect on the heat capacity and heat transfer coefficient, since a very small fraction of the fluid flows between louver passages. On the other hand, louver directed flow has a positive impact on the heat transfer coefficient. In the current study, flow efficiency is

[5] For F_p =1.5, θ=60, third-order upwind biased scheme with a TVD type limiter had to be applied to maintain a stable solution.

defined to be the ratio of mean flow angle (α_{mean}), which is obtained by averaging flow angles through out the louver bank (inlet, redirection and exit louvers are not included), to louver angle (θ) as follows:

$$\eta = \frac{\alpha_{mean}}{\theta} \tag{4}$$

The average normal velocity across top boundary to that across the left boundary is used to define flow angle in an individual block surrounding a louver, as follows:

$$\alpha = \tan^{-1} \frac{\int v dx / L_P}{\int u dy / F_P} \tag{5}$$

The friction factor (Fanning) is defined as:

$$f = \frac{2 \cdot \Delta p \cdot D_H}{4 \cdot F_d \cdot V_c^2} \tag{6}$$

where Δp is the pressure drop across the fin in the flow direction, D_h is the hydraulic diameter, F_d is the flow depth, and V_c is the maximum mean velocity.

The dimensional heat flux on the louver surface is defined

$$q^* = -k \frac{\partial T^*}{\partial n^*} = h^* (T_f^* - T_{ref}^*) \tag{7}$$

where n^* is measured along the normal to the louver surface, and T_{ref}^* is a reference temperature. Non-dimensionalizing the above equation gives

$$Nu^2 = \frac{h^* L_p^*}{k} = \frac{-\partial T / \partial n}{(1 - T_{ref})} \quad \text{and} \quad q = \frac{q^* L_p^*}{k(T_f^* - T_{in}^*)} = -\frac{\partial T}{\partial n} \tag{8}$$

When $T_{ref} = T_{in} = 0$, we define a local Nusselt number on the louver surface as

$$Nu^1 = q = -\frac{\partial T}{\partial n} \tag{9}$$

which is identical to the non-dimensional heat flux. When T_{ref} is the mixed mean temperature calculated as:

$$T_{ref} = T_{mean} = \frac{\sum_{F_p, F_d} |u| T \Delta y}{\sum_{F_p, F_d} |u| \Delta y} \tag{10}$$

the heat transfer coefficient Nu^2 is obtained. Based on the above definition we define the average heat transfer coefficient for the whole fin, $< Nu^2 >_{fin}$.

2.4 Results and Analysis

Table 2.1 summarizes the cases simulated. Louver angles ranging from θ=20 to 60 degrees are studied for two large fin pitch ratios, F_p = 1.5 and 2.0, at Reynolds numbers Re_{in} = 50, 100, 200, and 300. Most of the cases are

steady, however as the louver angle increases the steady separation zones becomes unstable with periodic vortex shedding. At $\theta = 60°$, the flow is unsteady for $Re_{in} \geq 200$, and for $\theta = 40°$, initial instabilities appear at $Re_{in}=300$. For unsteady flows, time averaged results are presented.

Table 2.1: Summary of louver geometries studied.

Case	F_p	θ	b	F_d	S_1	S_3	S_2
1	1.5	25	0.1	13	1.0	0.5	1.0
2		30					
3		40					
4		50					
5		60					
6	2.0	25	0.1	13	1.0	0.5	1.0
7		40					
8		50					
9		60					

Figure 2.2 shows the distribution of the time-averaged temperature contours at F_p =1.5 for six cases at two Reynolds numbers and three louver angles. At Re_{in} = 50, as the louver angle increases, the flow gradually changes from duct directed to louver directed increasing the flow efficiency. At Re_{in} = 200, temperature contours are already well aligned with the louver direction indicating a high flow efficiency. As the louver angle increases further, its effect on aligning the flow with the louver is incremental and not as dramatic as at the lower Re_{in} = 50. In fact at θ=60° Re_{in} = 200, louvers after the re-direction louver exhibit flow that is more duct directed than in the direction of louvers. Not only does the flow efficiency impact the amount of fluid moving through the louver, it also influences thermal wake interactions between louvers. Thermal wakes of upstream louvers impinging on downstream louvers have a large effect on the heat transfer coefficient [4]. Duct flow is strongly related to intra-fin interference, which occurs between louvers in the same fin, [case (a)]. Inter-fin interference occurs between adjacent rows of fins when the flow is louver directed [case (e)]. Intra-fin interference is much stronger than inter-fin and has a large detrimental effect on heat transfer coefficient. Hence, to first order, it is reasonable to assume that higher flow efficiencies usually result in higher heat transfer coefficients, barring other effects.

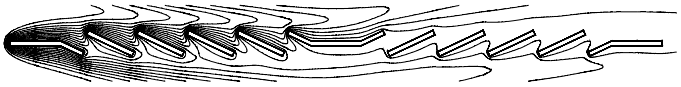

(a) θ = 25°, Re = 50

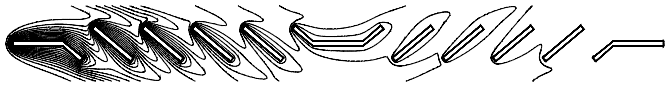

(b) *θ = 40°, Re = 50*

(c) *θ = 60°, Re = 50*

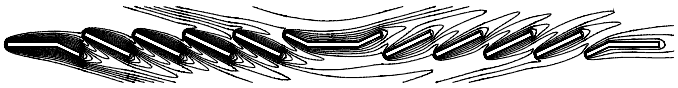

(d) *θ = 25°, Re = 200*

(e) *θ = 40°, Re = 200*

(f) *θ = 60°, Re = 200*

Figure 2.2: Distribution of the time-averaged temperature contours (F_p = 1.5).

Figure 2.3 shows the effect of louver angle θ on flow efficiency η. It is clear that F_p = 1.5 usually results in higher flow efficiency than F_p = 2.0. In general increasing the flow angle θ has a positive effect on flow efficiency up to $Re_{in} \leq 100$, after which increasing θ has a detrimental effect. At Re_{in} = 50, η increases as the louver angle increases for both F_p = 1.5 and 2.0. When Re_{in} > 100 and F_p = 1.5, η reaches a maximum value at θ=50°, and subsequently reduces slightly at θ=60°. A similar trend is evident for F_p = 2.0. At Re_{in} = 100, for F_p = 2.0, η achieves a maximum value earlier at θ=40°; for Re_{in} = 200 and 300, however, η decreases as θ increases.

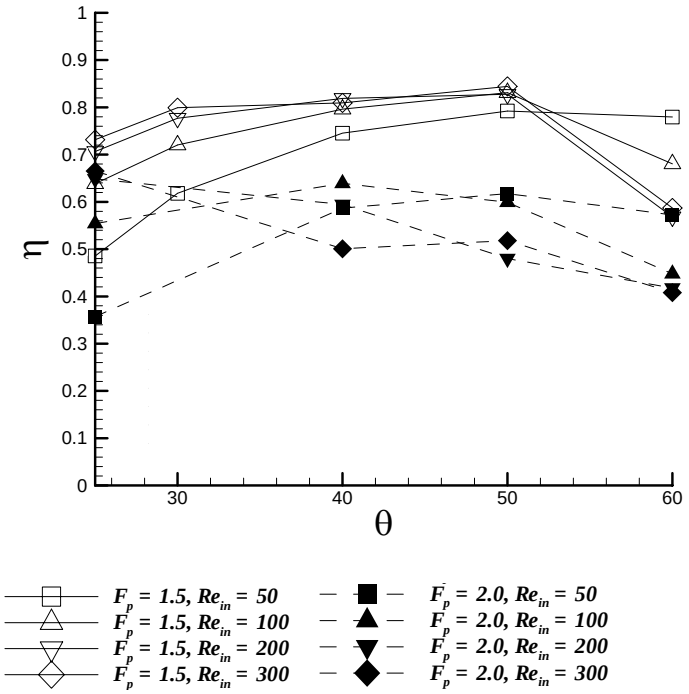

Figure 2.3: Effect of louver angle on flow efficiency.

Figure 2.4 shows the effect of louver angle θ on heat transfer coefficient $<Nu^2>_{fin}$. With other parameters fixed, $<Nu^2>_{fin}$ increases monotonically with θ and Re_{in} with the heat transfer coefficient being larger at F_p = 1.5 than at F_p = 2.0. At a Reynolds number of 300 and θ>40°, there is a noticeable change in slope as a consequence of the developing unsteadiness. The fact that the heat transfer coefficient increases in spite of the flow efficiency decreasing in some cases is unexpected and is investigated further.

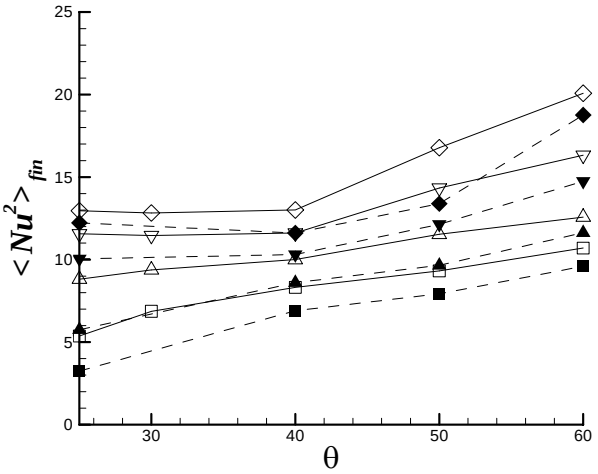

Figure 2.4: Effect of louver angle on heat transfer coefficient $<Nu^2>_{fin}$. See Figure 2.3 for legend.

Figure 2.5 shows the effect of louver angle θ on friction coefficient f. Similar to the heat transfer coefficient, the friction coefficient f increases as θ increases. Most of the increase comes from an increase in form drag. Again, there is a noticeable increase in the slope once the flow becomes unsteady with vortex shedding.

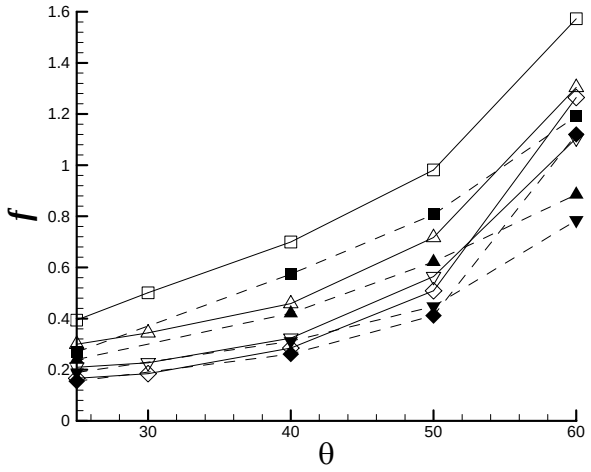

Figure 2.5: Effect of louver angle on friction factor f. See Figure 2.3 for legend.

Figure 2.6 shows the streamlines for three cases (a) θ = 25°, Re_{in} = 200, (b) θ = 60°, Re_{in} = 50 and (c) θ = 60°, Re_{in} = 200. In case (a) θ = 25°, Re_{in} = 200, the flow is vectored well by the louvers and passes through the louvers. In case (b) θ = 60°, Re = 50, recirculation zones appear on the lee side of some louvers, such as the second, sixth and eleventh louver. In case (c) θ = 60°, Re = 200, however, large unsteady separation zones are present at most of the louvers, especially downstream of the re-direction louver. These large recirculation zones block the flow between louvers and reduce the flow efficiency. Figure 2.7 plots the louver by louver distribution of the flow angle for these three cases. The local flow angle in case (a) does not change much with louver number and varies between 16° and 19°. In case (b), the flow angle increases from 41° at the second louver to 52° at the fifth louver. The flow angle then reduces to 35° at the seventh louver and then increases again to 52° at the tenth louver. In case (c), however, the flow angle changes drastically. The flow angles are 35°, 52°, 47° and 57° for the first four louvers, respectively, but reduce to 24°, 13°, 24° and 13° for the last four louvers as a result of the flow blockages caused by the large recirculation zones. Hence the average flow efficiency is lower at Re_{in} = 200 than at Re_{in} = 50 for θ = 60°.

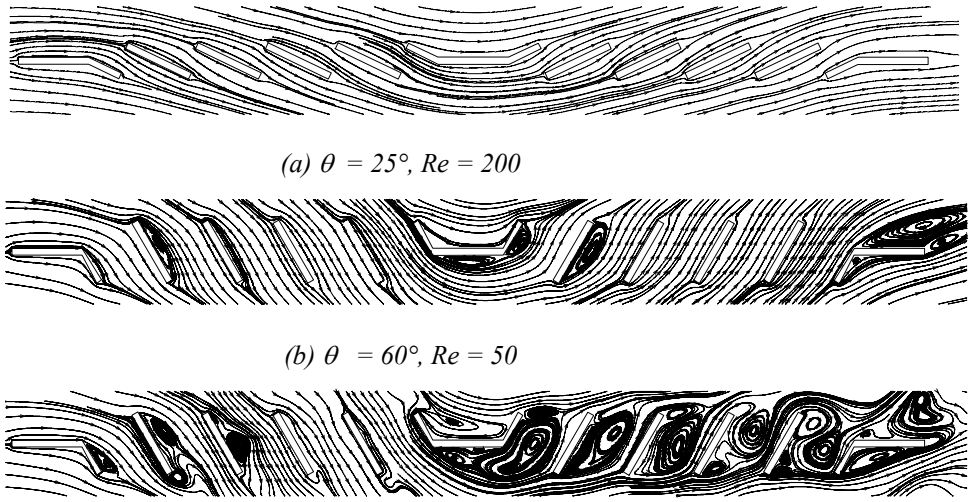

(a) θ = 25°, Re = 200

(b) θ = 60°, Re = 50

(c) θ = 60°, Re = 200

Figure 2.6: Instantaneous streamline patterns (F_p = 1.5).

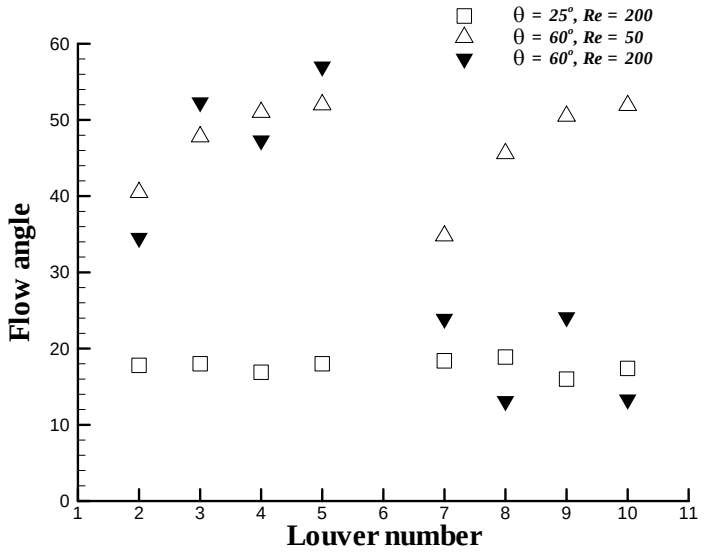

Figure 2.7: Louver-by-louver distribution of flow angles for the three cases shown in Figure 2.6 (F_p = 1.5).

Figure 2.8 illustrates the leading and trailing surfaces of the louvers. For louvers before the re-direction louver, bottom surfaces are leading surfaces, while for the louvers after the re-direction louver, the top surfaces are leading. Figure 2.9 plots the heat flux along the leading and trailing surfaces of louvers 3, 4, 8 and 9 for two louver angles $\theta = 40°$ and $\theta = 60°$ at $Re_{in} = 200$ and F_p = 1.5. The distance s has its origin at the leading edge of the louver, and its range is from 0.0 to 1.0 along the length of the louver. It is found that the heat flux Nu^l on the leading surface is much higher than that on the trailing surface, especially at the leading edge of the louver. In addition, Nu^l on the leading surface increases dramatically when the louver angle θ increases from $40°$ to $60°$. This is a consequence of a combination of flow impingement and the shear induced by the presence of large recirculation

zones. The recirculating zones by virtue of their rotational motion draw in fluid from the freestream which impinges on the leading edge and thins the thermal boundary layer. Conversely, the recirculation region does not give access to freestream fluid on the trailing surface and as a result, the heat flux on the trailing surface does not change as much as that on the leading surface.

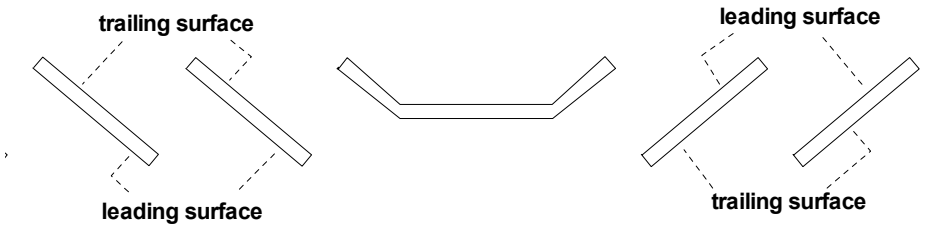

Figure 2.8: Illustration of the leading and trailing surface of the louvers.

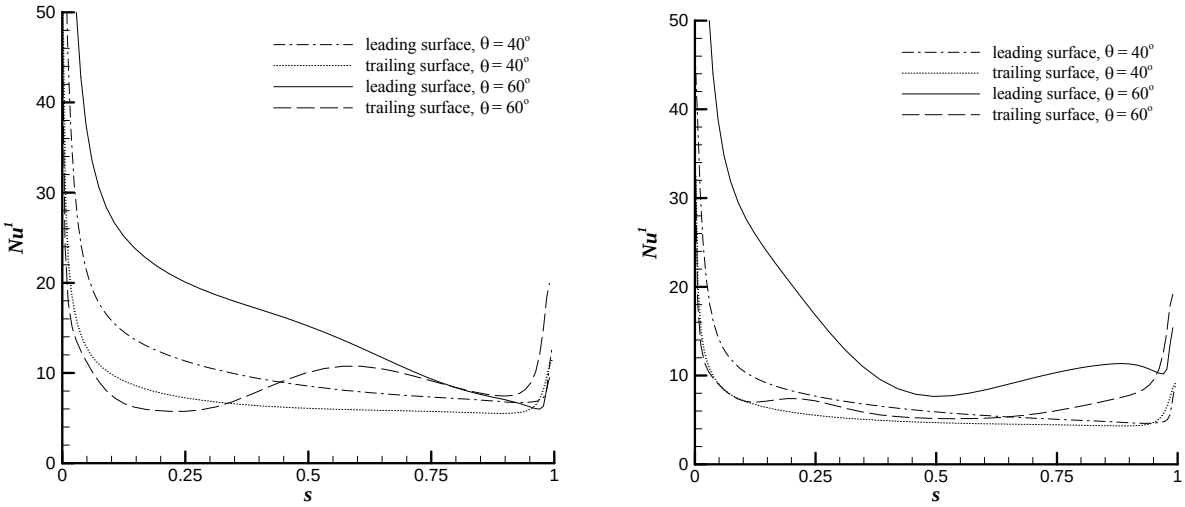

(a) Louver 3 (b) Louver 4

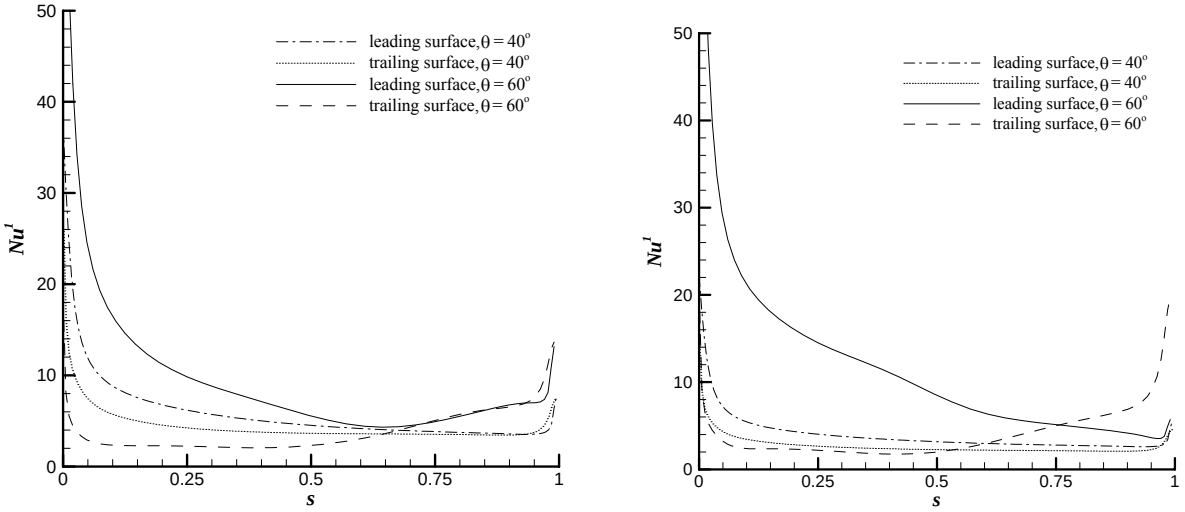

(c) Louver 8 (d) Louver 9

Figure 2.9: Local distribution of non-dimensional heat flux on the leading and trailing surfaces of selected louvers. (Re_{in} = 200 and F_p = 1.5)

Figure 2.10 plots the variation of the averaged heat flux on the leading and trailing surfaces for the whole fin (excluding the entrance, re-direction, and exit louvers) with louver angle for two cases Re_{in} =*50* and *200*. It shows that the average heat flux $\overline{Nu}^1$ on the leading surface is higher than that on the trailing surface, except in the case θ = *25°* and *30°, Re_{in} = 50*, and it increases very quickly with higher louver angle while $\overline{Nu}^1$ on the trailing surface is fairly constant. As noted previously, as the flow angle increases, the action of flow impingement with and without the presence of recirculating zones on the leading surface of louvers becomes a dominant mode of heat transfer. For example louvers 3 and 4 in Figs. (6&9) experience direct impingement, whereas louvers 8 and 9 experience impingement which is aided by the circulatory motion of the large recirculation zones present. Hence, in

spite of a decrease in flow efficiency, the augmentation provided by flow impingement as the louver angle increases, increases the overall heat transfer coefficient. At $\theta = 25°$ and 30° at Re=50, the trends are opposite. This is a result of thermal wake interference on the leading sides which lowers the heat flux, whereas the trailing surfaces are relatively free of these effects. At low angles and low Reynolds numbers, because the flow is directed in the streamwise direction, the thermal wake from upstream louvers interferes and lowers the heat transfer on the leading side of louvers. As the angle and Reynolds number increase, the flow becomes more louver directed and thermal wake effects on the leading side decrease, whereas impingement effects increase.

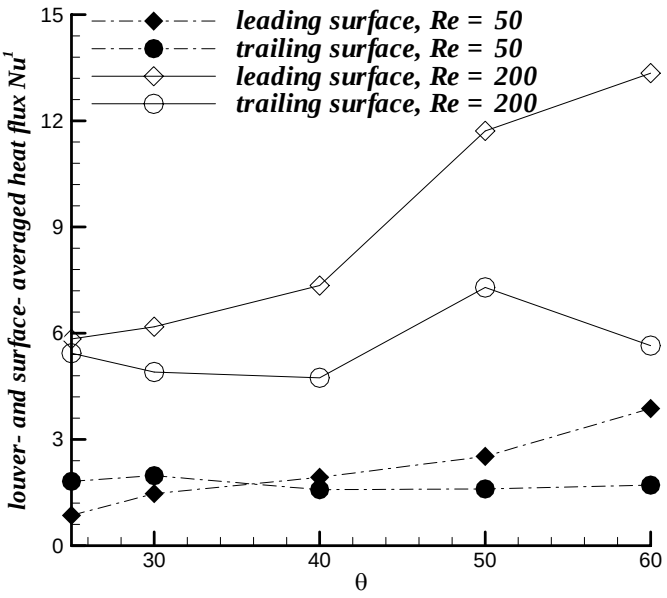

Figure 2.10: Variation of fin-averaged heat flux on the leading and trailing surfaces with louver angle θ (F_p = 1.5).

2.5 Summary and Conclusions

The paper evaluates the use of large louver angles with large fin pitch multilouvered fins. Two fin pitches, F_p = 1.5 and 2.0 are studied for louver angles ranging from 20 to 60 degrees. The effect of louver angle on flow efficiency, friction, and heat transfer is reported for Reynolds numbers less than 500.

The numerical results show that when the louver angle is increased, both the heat transfer coefficient and friction coefficient increase. The flow efficiency has an optimal value near 50° when the Reynolds number is less than 100, and then decreases with a further increase in louver angle. As the Reynolds number increases further, the flow efficiency starts decreasing at lower louver angles. The decrease is primarily a result of recirculation zones forming in the wake of louvers, which behave as blockages. Contrary to expectations, in spite of the flow efficiency decreasing, both heat transfer and friction coefficients increase monotonically with an increase in louver angle.

The increase in heat transfer coefficients in spite of a drop in flow efficiency is found to be a result of enhancement provided by flow impingement, both direct and that induced by recirculating fluid, on the leading

surface of louvers. As louver angle increases impingement heat transfer becomes a dominant mode of heat transfer augmentation.

Hence, large louver angles can be used to augment heat transfer at low Reynolds numbers and large fin pitches at the price of a larger system pressure drop.

2.6 References

1. Davenport, C. J., Heat Transfer and Flow Friction Characteristics of Louvered Heat Exchanger surfaces, Heat Exchangers: Theory and Practice, Taborek, J., Hewitt, G. F. and Afgan, N. (eds.), pp. 397-412, Hemisphere, Washington, D. C., 1983.
2. Webb, R. L. and Trauger, P., Flow Structure in the Louvered Fin Heat Exchanger Geometry, *Experimental Thermal and Fluid Science*, 4, pp. 295 - 217, 1991.
3. Tafti D. K. and Zhang, X., Geometry Effects on Flow Transition in Multilouvered Fins - Onset, Propagation, and Characteristic Frequencies, *Int. J. Heat Mass Transfer*, 44, pp. 4195-4210, 2001.
4. Zhang, X. and Tafti, D. K., Classification and Effects of Thermal Wakes in Multilouvered Fins, *Int. J. Heat Mass Transfer*, 44, pp. 2461-2473, 2001.
5. Achaichia, A. and Cowell, T. A., A Finite Difference Analysis of Fully Developed Periodic Laminar Flow in Inclined Louvered Arrays, Proceedings of 2nd UK National Heat Transfer Conference, Glasgow, Vol. 2, pp. 883-888, 1988.
6. Achaichia, A. and Cowell, T. A., Heat Transfer and Pressure Drop Characteristics of Flat tube and Louvered Plate Fin Surfaces, *Experimental Thermal and Fluid Science*, Vol. 1, pp. 147-157, 1988.
7. Antoniou, A. A., Heikal, M. R., and Cowell, T. A., Measurements of Local Velocity and Turbulence Levels in Arrays of Louvered Plate Fins, Heat Transfer 1990, Vol. 4, pp. 105-110, 1990.
8. Sahnoun, A. and Webb, R. L., Prediction of Heat Transfer and Friction for the Louver Fin Geometry, *J. Heat Transfer*, Vol. 114, pp. 893-900, 1992.
9. Dillen, E. R. and Webb, R. L., Rationally Based Heat Transfer and Friction Correlations for the Louver Fin Geometry, SAE paper 950504, Detroit, 1994.
10. Springer, M. E. and Thole, K. A., Entry Region of louvered fin Heat Exchangers, *Experimental Thermal and Fluid Science,* 19 (1999), pp. 223 - 232.
11. Baldwin, S. J., White, P. R. S., Al-Daini, A. J. and Davenport, C. J., Investigation of the Gas Side Flow Field in Multilouver Ducts with Flow Reversal, 5th Int. Conf. on Numerical Methods in Laminar and Turbulent Flow, Montreal, Vol. 5, Pt. 1, pp. 482-495, 1987.
12. Suga, K., Aoki, H. and Shingawa, T., Numerical Analysis on Two-Dimensional Flow and Heat Transfer of Louvered Fins Using Overlaid Grids, *JSM International Journal*, Vol. 33, pp. 122-127, 1989.
13. Suga, K. and Aoki, H., Numerical Study on Heat Transfer and Pressure Drop in Multilouvered Fins, *ASME/JSME Thermal Engineering Proceedings*, Vol. 4, pp. 361-368, 1991.
14. Hiramatsu, M., Ishimaru, T. and Matsuzaki, K., Research on Fins for Air Conditioning Heat Exchangers, *JSME International Journal*, Vol. 33, pp. 749-756, 1990.
15. Achaichia, A., Heikal, M. R., Sulaiman, Y. and Cowell, T. A., Numerical Investigation of Flow and Friction in Louver Fin Arrays. 10th Int. Heat Transfer Conf., Heat Transfer 1994, Vol. 4, pp. 333-338, 1994.
16. Bellows, K. D., Flow Visualization of Louvered-Fin Heat Exchangers, M.S. Thesis, Department of Mechanical and Industrial Engineering, University of Illinois at Urbana Champaign, 1996.
17. DeJong, N. C. and Jacobi, A. M., Flow, Heat Transfer, and Pressure Drop Interactions in Louvered-Fin Arrays, ACRC TR-146, University of Illinois Urbana Champaign, 1999.

18. Tafti, D. K., Zhang L. W., and Wang, G., A Time-Dependent Calculation Procedure for Fully Developed and Developing Flow and Heat Transfer in Louvered Fin Geometries, *Num. Heat Transfer A,* 35(3), pp.225-249, 1999.

19. Tafti, D. K., Wang G. and Lin W., Flow Transition in a Multilouvered Fin Array, *Int. J. Heat Mass Transfer*, vol. 43, No. 6, pp. 901-919, 2000.

20. Cui, J. and Tafti, D. K., Computations of flow and heat transfer in a three-dimensional multilouvered fin geometry, *Int. J. Heat Mass Transfer,* 45, pp. 5007-5023, 2002.

21. Tafti, D. K. and Cui, J., Fin Tube Junction Effects on Flow and Heat Transfer in Flat Tube Multilouvered Heat Exchangers, *Int. J. Heat Mass Transfer*, 45(25), pp. 5007-5023, 2002.

22. Tafti, D. K. and Cui, J., Advances in Computations of Air-Side Heat Transfer in Compact Heat Exchangers, invited, Proceedings of IMECE2002, Vol. 1, Heat Transfer-2, paper no. IMECE2002-32830, Nov. 2002.

23. Zhang, X. and Tafti, D. K., Flow efficiency in multi-louvered fins, *Int. J. Heat Mass Transfer,* 46(10), pp. 1737-1750, 2003.

Chapter 3. Effect of Inlet Flow Angle on Performance

Abstract

The effect of inlet flow angles on flat tube multilouvered fin heat exchangers is studied. Five inlet flow angles, $\alpha = \pm 25, \pm 45$ and 0 degrees are employed with respect to the face of the heat exchanger. One louver angle θ = 25 degrees, and three fin pitches, F_p =1.0, 1.5 and 2.0 are considered. There is a strong correlation between the response of the flow efficiency and heat transfer coefficient to inlet flow angle. Positive flow angles, which are in the same direction as the louver angle, have to undergo a smaller rotation to be aligned with louver directed flow in the bank, and exhibit better performance characteristics than negative inlet flow angles. The first-order effect of inlet flow angles is to reduce the effective mass flow rate and Reynolds number through the heat exchanger. For positive flow angles and small fin pitches, the heat transfer coefficient correlates well with the effective Reynolds number $\{Re_{eff} = Re(\cos\alpha)\}$. However, this is not the case when flow angles are negative and the fin pitch increases. Under these conditions, the Nusselt number deviates considerably from the effective Reynolds number analogy, with a subsequent loss in heat transfer capability. For large negative inlet flow angles (α = -45), the heat transfer coefficient drops as much as 50% for a fin pitch F_p = 2.

Nomenclature

$\vec{a^j}$	contravariant basis vectors
b	fin thickness,
F_p	non-dimensional fin pitch,
F_d	non-dimensional flow depth,
$\sqrt{g}$	Jacobian of transformation
g^{jk}	contravariant metric tensor
k	thermal conductivity,
L_p^*	dimensional louver pitch (characteristic length scale),
Nu^1	non-dimensional heat flux,
Nu^2	non-dimensional heat transfer coefficient,
Pr	Prandtl number,
q	non-dimensional heat flux,
Re_{in},Re	Reynolds number,
T	temperature,
u_i	Cartesian velocity vector
U^j	Contravariant velocity components

Greek symbols

α	inlet flow angle,
β	flow angle in louver bank
η	flow efficiency,
v	kinematic viscosity,
θ	louver angle.

Superscripts

*	dimensional quantities.

Subscripts

f, fin based on fin.

3.1 Introduction

Multi-louvered fin compact heat exchangers are used extensively in the automobile, heating, ventilation and air-conditioning industries. A typical flat-tube louvered heat exchanger with rectangular channels is shown in Figure 3.1(a). Three important factors affect the heat transfer capacity in multi-louvered geometries; they are (a) the dominant flow direction [1, 2], or flow efficiency, (b) the presence of flow unsteadiness and associated large-scale structures [3], and (c) thermal wake interference [4].

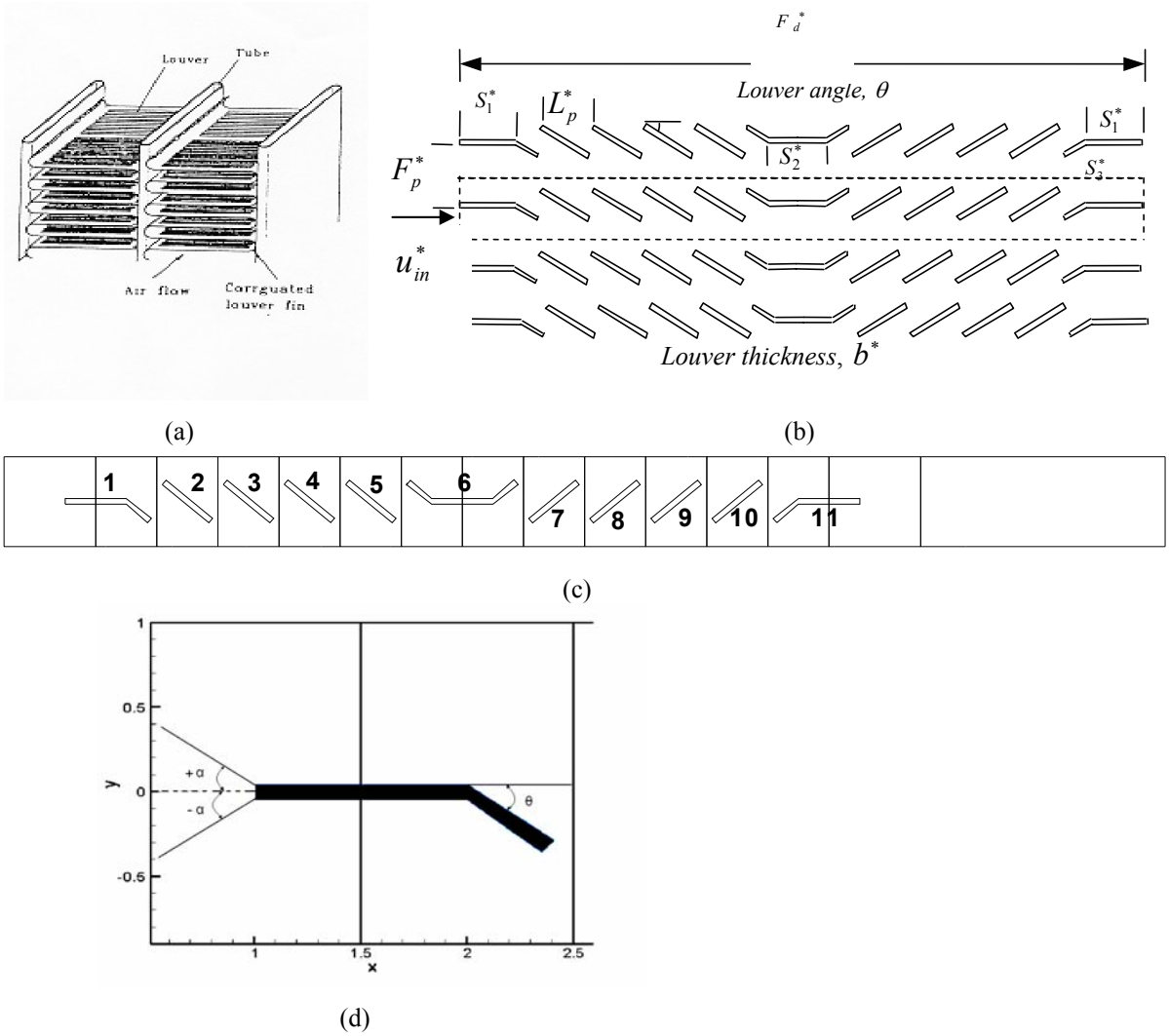

Figure 3.1. (a) Flat tube louvered heat exchanger; (b) Cross-section of multi-louvered fin array. Dotted lines show the basic computational unit; (c) Multi-block domain decomposition; (d) Nomenclature used to define inlet flow angle.

Early experimental studies established the basic flow structure in multilouvered fins and also measured the heat transfer coefficient. Davenport [1] identified that at low Reynolds number there was a flattening of the *j*-factor curve, which he attributed to the transition to duct directed flow. Achaichia and Cowell [5], numerically studied an

infinite array of zero thickness louvers and derived an expression for flow angle from their results. In a related study, Achaichia and Cowell [6] reported heat transfer and friction data for 23 sample geometries. Antoniou et al. [7] made turbulent measurements in a louvered fin. Subsequently Webb and his group [2,8,9] also investigated louvered fins. They developed a correlation for flow efficiency based on their data and found that it did not agree with the correlations of Achaichia and Cowell [5]. Springer and Thole [10] found that larger fin pitches resulted in lower average flow angles in the louver passages and longer development lengths. DeJong and Jacobi [11] performed an experimental investigation on pressure drop and heat transfer.

Several computational studies of multi-louver geometries have been attempted since the 1980s. Various simplifying assumptions made in earlier studies have prevented the use of computations for complete and reliable predictions of multi-louvered fins. These studies assumed louvers of zero thickness and/or fully-developed flow conditions [5], and/or Cartesian grids with a staircase louver surface [12]. Later, Suga et al. [13] and Suga and Aoki [14] used overlaid grids for representative multi-louvered fins. Hiramatsu at al. [15] used oblique or body-fitted grids in the calculation domain. Achaichia et al. [16] studied the flow pattern in multi-louvered fins with the commercial code PHOENICS along with the k-ε turbulence model for high Reynolds numbers.

Tafti et. al. [3, 4, 17-18] have applied time-dependent calculations to two-dimensional multi-louvered geometries. Two fin pitch to louver pitch ratios and four louver angles were studied, in addition to the effect of fin thickness. Zhang and Tafti [19] used over two-hundred high resolution simulations to develop a correlation for flow efficiency. Cui and Tafti [20] and Tafti and Cui [21, 22] extended the numerical modeling to three-dimensional aspects of the louver geometry near the louver-tube junction.

In many applications of multi-louvered heat exchangers the operating Reynolds number seldom increases beyond 500 based on the face velocity and louver pitch. Although multi-louvered fins have been studied extensively in the past two decades, little attention has been given to the low Reynolds number flow regime, partly because of the increased experimental uncertainties experienced in measuring pressure drops and heat transfer. In this range of Reynolds numbers, heat transfer capacity is quite dependent on the direction of flow or flow efficiency. Also to the best of our knowledge, no studies have critically evaluated the effect of inlet flow angle on performance – all studies assume that the flow is normal to the heat exchanger face. This is not the case when a louvered heat exchanger is placed in the wake of another. Depending on the orientation of the outlet louver, the flow assumes an angle and will not be normal to the face of the downstream exchanger. In many instances, the heat exchanger itself maybe tilted for better condensate drainage.

Our objective in this paper is to evaluate the effect of inlet flow angle on heat transfer performance. Five flow angles, α = -45, -25, 0, +25 and +45 degrees are studied with three fin pitches F_p = 1.0, 1.5 and 2.0 and a louver angle of 25 degrees. Three Reynolds numbers, 100, 300, and 500 are investigated.

3.2 Computational Details

The Navier-Stokes and energy equations are mapped from physical $(\vec{x})$ to logical/computational space $(\vec{\xi})$ by a boundary conforming transformation $\vec{x} = \vec{x}(\vec{\xi})$, where $\vec{x} = (x,y,z)$ and $\vec{\xi} = (\xi,\eta,\zeta)$. The transformed

non-dimensional time-dependent incompressible Navier-Stokes and the energy equations in computational space are written in strong-conservative form as:

Continuity:

$$\frac{\partial}{\partial \xi_j}\left(\sqrt{g}U^j\right)=0 \tag{1}$$

Momentum:

$$\frac{\partial}{\partial t}\left(\sqrt{g}u_i\right)+\frac{\partial}{\partial \xi_j}\left(\sqrt{g}U^j u_i\right)=-\frac{\partial}{\partial \xi_j}\left(\sqrt{g}(\overrightarrow{a^j})_i\, p\right)+\frac{\partial}{\partial \xi_j}\left(\frac{1}{\mathrm{Re}}\sqrt{g}g^{jk}\,\frac{\partial u_i}{\partial \xi_k}\right)+\sqrt{g}S_{u_i} \tag{2}$$

Energy:

$$\frac{\partial}{\partial t}\left(\sqrt{g}T\right)+\frac{\partial}{\partial \xi_j}\left(\sqrt{g}U^j T\right)=\frac{\partial}{\partial \xi_j}\left(\frac{1}{\mathrm{Pr}\,\mathrm{Re}}\sqrt{g}g^{jk}\,\frac{\partial T}{\partial \xi_k}\right)+\sqrt{g}S_T \tag{3}$$

The governing equations for momentum and energy conservation are discretized with a conservative finite-volume formulation. Both, convection and viscous terms are approximated by second-order central-difference schemes in a non-staggered arrangement. The computational unit, shown in Figure 3.1 (b) by the dotted lines, consists of one entire row of the louvered fin geometry allowing the inclusion of entrance and exit effects in the flow direction. Periodic boundary conditions are applied in the transverse direction while Dirichlet boundary conditions are specified at the entrance to the louver bank. The application of periodicity simulates a bank of louvers in the transverse direction.

The governing equations are non-dimensionalized by a characteristic length given by the louver pitch L_p^*, a characteristic velocity scale given by the inlet velocity to the array (u_{in}^*) and a temperature scale given by ($T_f^* - T_{in}^*$), where T_f^* is the specified fin surface temperature. The non-dimensionalization results in a characteristic Reynolds number $\mathrm{Re} = \mathrm{Re}_{in} = u_{in}^* L_p^* / \nu$, with Dirichlet boundary conditions $u_{in} = 1, T_{in} = 0$ at the entrance to the computational domain. The Prandtl number is fixed at 0.7 for air. At the fin surface, no slip and no penetration boundary conditions for the velocity field, and $T_f = 1$ for the temperature field are applied. Due to the recovering nature of the flow at the array exit, convective outflow boundary conditions are applied at this boundary. Details about the time-integration algorithm, treatment of boundary and louver surface conditions, and validation of the computer program can be found in Tafti et al. [17].

The configuration used in these calculations consists of an entrance and exit louver with four louvers on either side of the center or redirection louver. For all the calculations in this paper the louver thickness is fixed at b = 0.1. For the entrance and exit louvers, S_1 = 1, and for the center redirection louver, S_2 = 1. Figure 3.1(c) shows the computational domain which is resolved by 15 blocks, one for each louver, two each for the entrance, exit and redirection louver. The exit domain extends approximately 5.5 non-dimensional units (or 55 fin thicknesses) downstream of the array. Each block is resolved by 96x96 finite-volume cells (a total of 138,240 cells). This

resolution has been found to produce grid independent solutions at much higher Reynolds number than the ones simulated in this study.

3.3 Characterization Of Flow Efficiency, Friction, And Heat Transfer

Flow efficiency (η) is used to describe the percentage of the fluid flowing along the louver direction. A 100% efficiency represents ideal louver directed flow while 0% represents complete duct directed flow. High flow efficiencies generally result in higher heat transfer coefficients than low efficiencies. At low Reynolds numbers, heat transfer coefficients exhibit a strong dependence on flow efficiency. In the current study, flow efficiency is defined to be the ratio of mean flow angle (β_{mean}), which is obtained by averaging flow angles through out the louver bank (inlet, redirection and exit louvers are not included), to louver angle (θ) as follows:

$$\eta = \frac{\beta_{mean}}{\theta} \tag{4}$$

The average normal velocity across top boundary to that across the left boundary is used to define flow angle in an individual block surrounding a louver, as follows:

$$\beta = \tan^{-1} \frac{\int v dx / L_P}{\int u dy / F_P} \tag{5}$$

The friction factor (Fanning) is defined as:

$$f = \frac{2 \cdot \Delta p \cdot D_H}{4 \cdot F_D \cdot V_c^2} \tag{6}$$

where Δp is the pressure drop across the fin in the flow direction, D_h is the hydraulic diameter, F_d is the flow depth, and V_c is the maximum mean velocity.

The dimensional heat flux on the louver surface is defined

$$q^* = -k \frac{\partial T^*}{\partial n^*} = h^* (T_f^* - T_{ref}^*) \tag{7}$$

where n^* is measured along the normal to the louver surface, and T_{ref}^* is a reference temperature. Non-dimensionalizing the above equation gives

$$Nu = \frac{h^* L_p^*}{k} = \frac{-\partial T / \partial n}{(1 - T_{ref})} \quad \text{and} \quad q = \frac{q^* L_p^*}{k(T_f^* - T_{in}^*)} = -\frac{\partial T}{\partial n} \tag{8}$$

When $T_{ref} = T_{in} = 0$, we define a local Nusselt number on the louver surface as

$$Nu^1 = q = -\frac{\partial T}{\partial n} \tag{9}$$

which is identical to the non-dimensional heat flux.

The Nusselt number or non-dimensional heat transfer coefficient based on a reference temperature

$$h = Nu^2 = \frac{h^* L_p^*}{k} = \frac{-\partial T / \partial n}{(1 - T_{ref})} \tag{10}$$

is also defined, where T_{ref} is the mixed mean temperature calculated as:

$$T_{ref} = T_{mean} = \frac{\sum_{F_p, F_d} |u| T \Delta y}{\sum_{F_p, F_d} |u| \Delta y} \tag{11}$$

Based on the above definition we also define the average heat transfer coefficient for the whole fin, $< Nu^2 >_{fin}$.

3.4 Results and Analysis

Figure 3.1(d) illustrates the nomenclature used to define the inlet flow angle. When the flow angle is in the same direction as the louver angle it is denoted by a positive value or a negative value otherwise.

Figure 3.2(a-c) shows the average flow efficiency in the louver bank, the average Nusselt number or non-dimensional heat transfer coefficient, and the friction factor. Flow efficiency quantifies the average flow angle within the louver bank; higher the flow efficiency, larger is the flow alignment with the louver direction. Plotted on the *x*-axis is the inlet flow angle ranging from α = -45 to +45 degrees. The fin pitch, F_p is 1.0, 1.5, 2.0 and Re = 100, 300 and 500. The louver angle for all cases shown here is θ=25 degrees. The Nusselt numbers and friction factors for each case are normalized by the nominal value at zero flow angle.

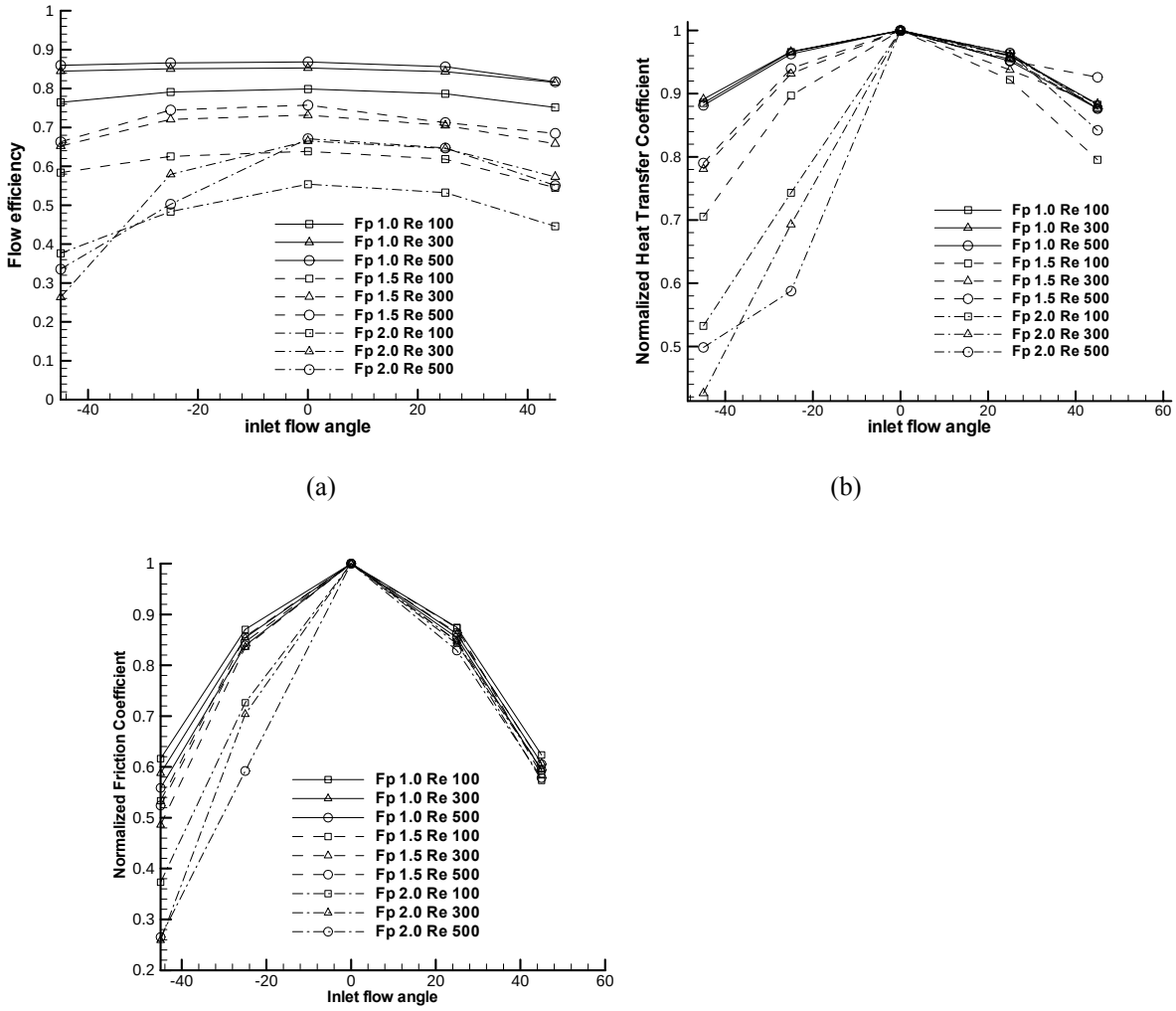

Figure 3.2. Variation of flow efficiency and normalized Nusselt numbers with inlet flow angles. Louver angle $\theta = 25$ degrees in all cases. Effect of inlet flow angle on flow efficiency, heat transfer coefficient, and friction factor is much stronger at large negative angles and large fin pitches.

The effect of inlet flow angle on the flow efficiency, friction, and heat transfer increases with fin pitch. There is a strong similarity between trends observed in flow efficiency and the Nusselt numbers. At a fin pitch of 1, inlet flow angle has a minimal effect (about -10%) on heat transfer coefficient and the orientation of the flow angle does not have a large effect. At fin pitches of 1.5 and 2.0, asymmetries start developing between the +ve and –ve flow angles. When the inlet flow angle is aligned to the inlet louver angle, the detrimental effect on heat transfer is confined to within -15 to -20% for a inlet angle up to +45 degrees. However, for flow angles not aligned with the louver angle, substantially greater losses in Nusselt numbers are incurred. These losses range from -20 to -30% for F_p =1.5 to greater than -50% for F_p = 2.0.

Similar trends are observed in the friction factor. However, contrary to expectations, the fractional drop in friction factor is much larger than the corresponding drop in the heat transfer coefficient. For positive flow angles,

the friction factor is between 50 to 60% of the value at zero incidence for all fin pitches and flow Reynolds numbers. For negative inlet flow angles, there is considerable variation between the different fin pitches; 50-60% for F_p =1 and 1.5, and 25-40% for F_p =2.

Examining the flow streamlines for F_p =1.5 and F_p =2.0 in Figure 3, it is found that as fin pitch increases, the ability of the flow to quickly align itself with the louvers decreases. This is true even at α=0. Hence, when a flow angle is imparted to the inlet stream, the ability of the stream to align with the louver deteriorates as the fin pitch increases. The flow distortion caused by the negative flow angles is much larger than when the flow angle is positive resulting in large separated zones at the entrance of the louver bank.

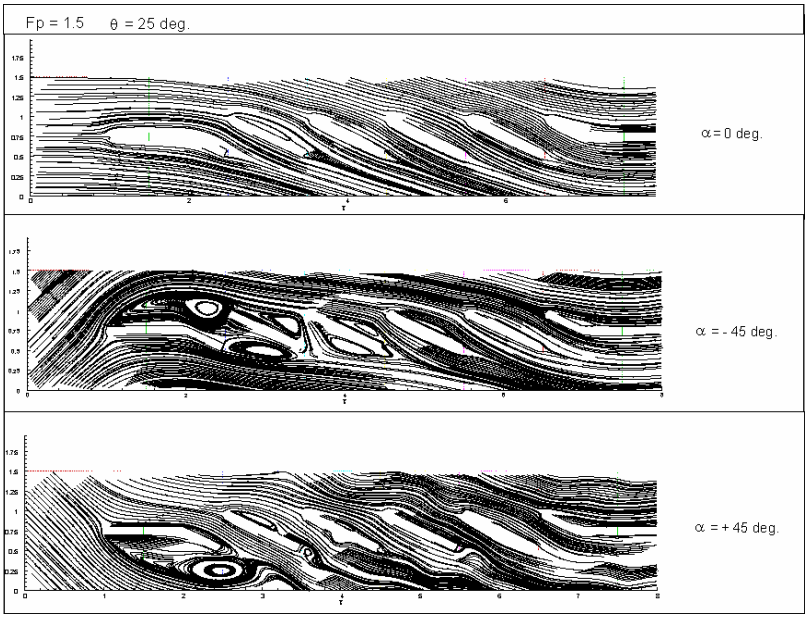

(a)

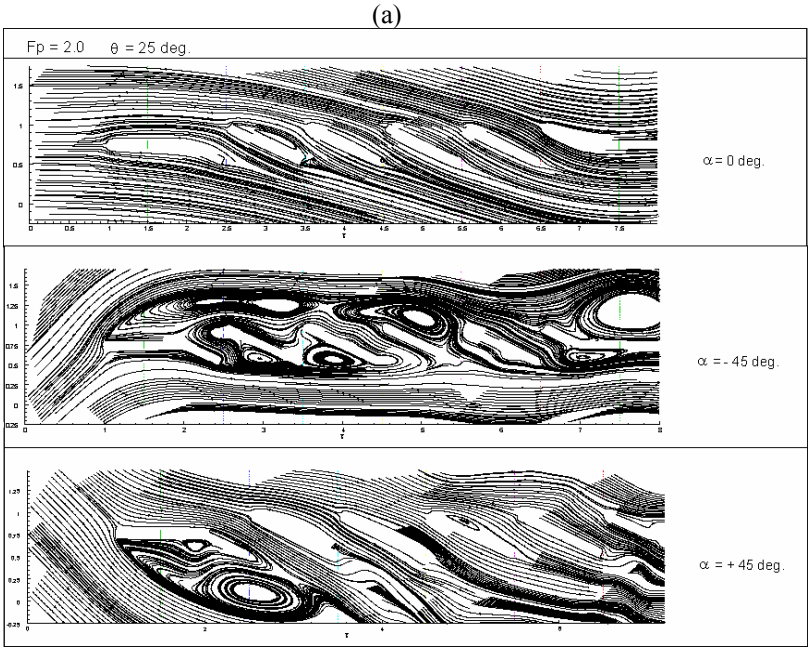

(b)

Figure 3.3. Streamline distribution in first half of louver bank at *Re*=500. (a) F_p=1.5; (b) F_p =2.0. Flow distortion is more intense at α = -45 and at F_p=2.

Figure 3.4 plots temperature contours in the louver bank at different inlet flow angles. The temperature closely reflects the flow efficiency and essentially follows the flow direction in the bank. The thermal wake characteristics change considerable with inlet flow angle. At α=-45 degrees, intra-fin wake (between louvers in the same fin) is the most dominant component but as the inlet flow angle tends to 0 and positive values, the wake components are more evenly distributed between intra- and inter (between fins) fin. As shown in [4], intra-fin wakes

which are a result of low flow efficiencies have a large effect on heat capacity and heat transfer coefficients, while inter-fin wakes do not.

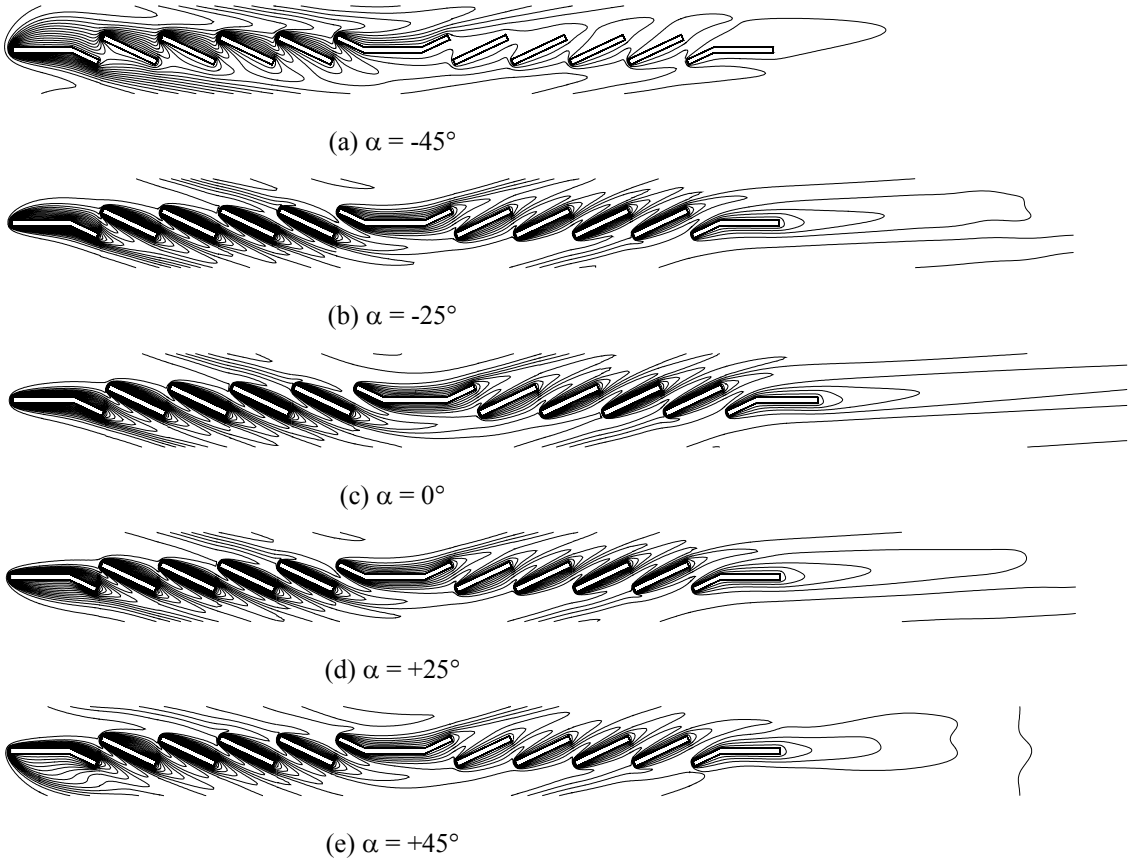

(a) α = -45°

(b) α = -25°

(c) α = 0°

(d) α = +25°

(e) α = +45°

Figure 3.4. Temperature contours at different inlet flow angles (F_p =1.5 & Re = 300). Thermal wake interference between louvers is much stronger at α = -45 degrees. As α assumes zero and positive values, wake interference decreases.

Figure 3.5 plots the louver-by-louver distribution of Nusselt number (or heat transfer coefficient) for F_p =2.0, for α = 0, +45, and -45 degrees. It is noted that the Nusselt number for α=-45 never quite recovers to the values at α=0 even downstream of the redirection louver. On the other hand, for α=+45, there is a quick recovery of the flow in the upstream half, but the values are lower downstream of the redirection louver.

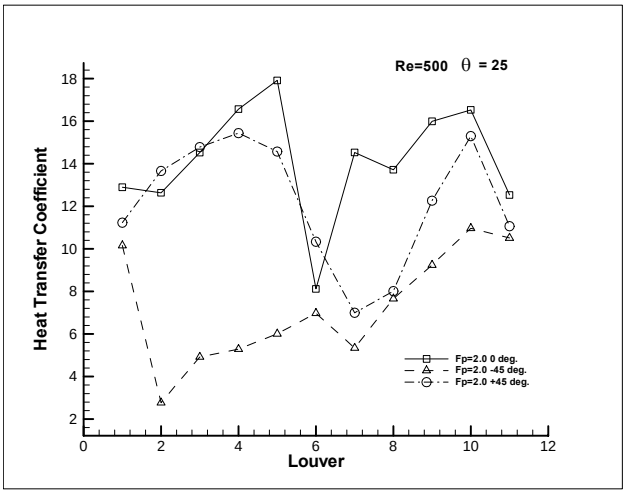

Figure 3.5. Effect of inlet flow angle on louver by louver distribution of Nusselt number. At α=-45 degrees, there is a sharp drop in the heat transfer coefficient in the first half of the louver bank.

Figure 3.6(a-b) shows the overall Nusselt number versus an effective Reynolds number, $Re_{eff} = Re(\cos\alpha)$. The inlet flow angle reduces the effective mass flux through the exchanger and hence to first order, in the absence of any non-linear effects, the Nusselt number should scale with Re_{eff}. The lines in 4(a-b) denote Nusselt numbers at α=0, while the symbols denote inlet flow angles. For F_p =1.0, irrespective of the orientation of the inlet flow, there is very good scaling when the Nusselt numbers are plotted against Re_{eff}. In both cases, the symbols match the solid lines quite well. As fin pitch increases to F_p =1.5 and 2.0, the Nusselt numbers still scale with Re_{eff} for the positive inlet angles. However, deviations increase as the fin pitch increases and the inlet flow angle increases, particularly as the inlet flow angle assumes larger negative values. Maximum deviations are found at F_p =2 and α=-45 degrees, in which non-linear flow effects dominate the heat transfer coefficient.

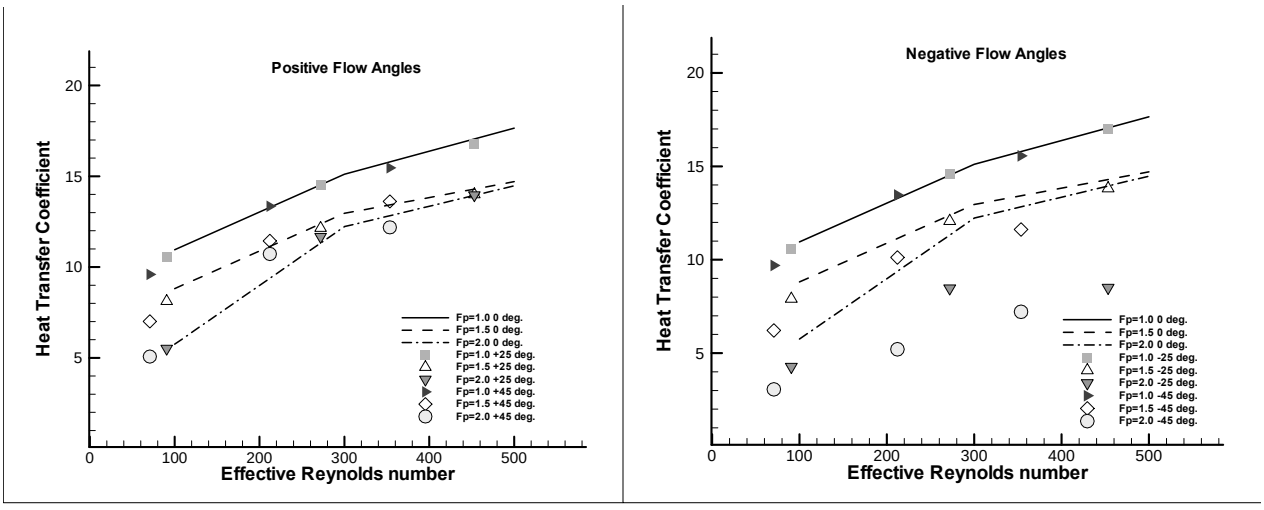

(a) (b)

Figure 3.6. Scaling of Nusselt numbers with effective Reynolds number $Re_{eff} = Re(\cos\alpha)$. Scaling holds for positive inlet flow angles and small fin pitches, but deteriorates as inlet flow angle assumes negative values and the fin pitch increases due to non-linear effects.

Figure 3.7(a-b) shows a modified friction factor (f_{mod}) plotted versus the effective Reynolds number. The modified friction factor is calculated based on an effective velocity in eqn. (6) and is given by $f_{mod} = f/\cos^2\alpha$. The nomenclature used is the same as Figure 3.6. The trends are similar to that observed in the heat transfer coefficient. For positive flow angles, f_{mod} scales well with the effective Reynolds number. However for negative inlet flow angles and large fin pitches, the scaling deteriorates considerably.

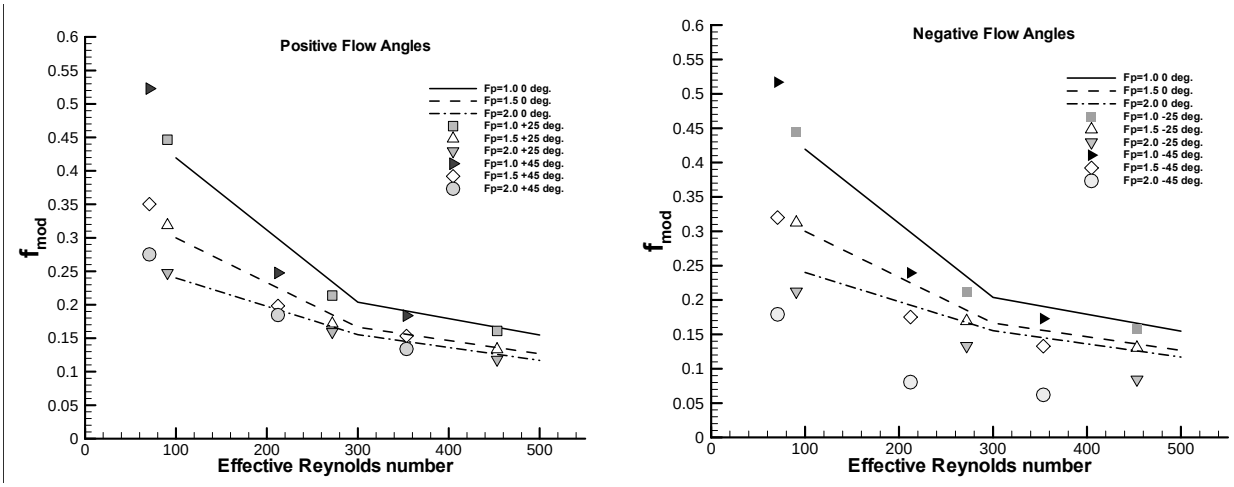

(a) (b)

Figure 3.7. Scaling of modified friction factor ($f_{mod} = f/\cos^2\alpha$) with effective Reynolds number $Re_{eff} = Re(\cos\alpha)$. Scaling holds for positive inlet flow angles and small fin pitches, but deteriorates as inlet flow angle becomes negative and fin pitch increases.

3.5 Summary and Conclusions

Results of developing flow and heat transfer in multi-louvered fins are presented for flows which are at an angle to the face of the heat exchanger. Five inlet flow angles ±25, ±45 and 0 degrees are employed with respect to the face of the heat exchanger. One louver angle $\theta = 25$ degrees, and three fin pitches, F_p =1.0, 1.5 and 2.0 are considered. Generally, positive angles exhibit better performance than the corresponding negative flow angle. This is because positive flow angles, which are in the same direction as the louver angle, have to undergo a smaller rotation to be aligned with louver directed flow in the bank. The first-order effect of inlet flow angles is to reduce the effective mass flow through the heat exchanger and hence the Reynolds number. This leads to an effective inlet Reynolds number which is smaller than the actual. For positive flow angles, and small fin pitches, the heat transfer coefficient correlates well with the effective Reynolds number. However, this is not the case when flow angles are negative. However, with an increase in fin pitch and inlet flow angles not aligned with the louver direction, the Nusselt number deviates considerably from the effective Reynolds number analogy, with a subsequent loss in heat transfer capability. At large negative inlet flow angles, the heat transfer coefficient drops as much as 50% for the fin pitch $F_p = 2$.

3.6 References

1. Davenport, C. J., Heat Transfer and Flow Friction Characteristics of Louvered Heat Exchanger surfaces, Heat Exchangers: Theory and Practice, Taborek, J., Hewitt, G. F. and Afgan, N. (eds.),pp. 397-412, Hemisphere, Washington, D. C., 1983.
2. Webb, R. L. and Trauger, P., Flow structure in the louvered fin heat exchanger geometry, Experimental Thermal and Fluid Science, 4, pp. 295 - 217, 1991.
3. Tafti D. K. and Zhang, X., Geometry Effects on Flow Transition in Multilouvered Fins - Onset, Propagation, and Characteristic Frequencies, Int. J. Heat Mass Transfer, 44, pp. 4195-4210, 2001.
4. Zhang, X. and Tafti, D. K., Classification and Effects of Thermal Wakes in Multilouvered Fins, Int. J. Heat Mass Transfer, 44, pp. 2461-2473, 2001.
5. Achaichia, A. and Cowell, T. A., A Finite Difference Analysis of Fully Developed Periodic Laminar Flow in Inclined Louvered Arrays, Proceedings of 2nd UK National Heat Transfer Conference, Glasgow, Vol. 2, pp. 883-888, 1988.
6. Achaichia, A. and Cowell, T. A., Heat Transfer and Pressure Drop Characteristics of Flat tube and Louvered Plate Fin Surfaces, Experimental Thermal and Fluid Science, Vol. 1, pp. 147-157, 1988.
7. Antoniou, A. A., Heikal, M. R., and Cowell, T. A., Measurements of Local Velocity and Turbulence Levels in Arrays of Louvered Plate Fins, Heat Transfer 1990, Vol. 4, pp. 105-110, 1990.
8. Sahnoun, A. and Webb, R. L., Prediction of Heat Transfer and Friction for the Louver Fin Geometry, J. Heat Transfer, Vol. 114, pp. 893-900, 1992.
9. Dillen, E. R. and Webb, R. L., Rationally Based Heat Transfer and Friction Correlations for the Louver Fin Geometry, SAE paper 950504, Detroit, 1994.
10. Springer, M. E. and Thole, K. A., Entry Region of louvered fin Heat Exchangers, Experimental Thermal and Fluid Science, 19, pp. 223 – 232, 1999.
11. DeJong, N. C. and Jacobi, A. M., Flow, Heat Transfer, and Pressure Drop Interactions in Louvered-Fin Arrays, ACRC TR-146, 1999.
12. Baldwin, S. J., White, P. R. S., Al-Daini, A. J. and Davenport, C. J., Investigation of the Gas Side Flow Field in Multilouver Ducts with Flow Reversal, 5th Int. Conf. on Numerical Methods in Laminar and Turbulent Flow, Montreal, Vol. 5, Pt. 1, pp. 482-495, 1987.
13. Suga, K., Aoki, H. and Shingawa, T., Numerical Analysis on Two-Dimensional Flow and Heat Transfer of Louvered Fins Using Overlaid Grids, JSM International Journal, Vol. 33, pp. 122-127, 1989.
14. Suga, K. and Aoki, H., Numerical Study on Heat Transfer and Pressure Drop in Multilouvered Fins, ASME/JSME Thermal Engineering Proceedings, Vol. 4, pp. 361-368, 1991.
15. Hiramatsu, M., Ishimaru, T. and Matsuzaki, K., Research on Fins for Air Conditioning Heat Exchangers, JSME International Journal, Vol. 33, pp. 749-756, 1990.
16. Achaichia, A., Heikal, M. R., Sulaiman, Y. and Cowell, T. A., Numerical Investigation of Flow and Friction in Louver Fin Arrays. 10th Int. Heat Transfer Conf., Heat Transfer 1994, Vol. 4, pp. 333-338, 1994.
17. Tafti, D. K., Zhang L. W., and Wang, G., A Time-Dependent Calculation Procedure for Fully Developed and Developing Flow and Heat Transfer in Louvered Fin Geometries, Num. Heat Transfer A, 35(3), pp. 225-249, 1999.
18. Tafti, D. K., Wang G. and Lin W., Flow Transition in a Multilouvered Fin Array, Int. J. Heat Mass Transfer, 43(6), pp. 901-919, 2000.
19. Zhang, X. and Tafti, D. K., Flow efficiency in multi-louvered fins, Int. J. Heat Mass Transfer, 46(10), pp. 1737-1750, 2003.
20. Cui, J. and Tafti, D. K., Computations of flow and heat transfer in a three-dimensional multilouvered fin geometry, Int. J. Heat Mass Transfer, 45(25), pp. 5007-5023, 2002.

21. Tafti, D. K. and Cui, J., Fin-Tube Junction Effects on Flow and Heat Transfer in Flat Tube Multilouvered Heat Exchangers, Int. J. Heat Mass Transfer 46(11), pp. 2027-2038, 2003.

22. Tafti, D. K. and Cui, J., Advances in Computations of Air-Side Heat Transfer in Compact Heat Exchangers, invited, Proceedings of IMECE2002, Vol. 1, Heat Transfer-2, paper no. IMECE2002-32830, Nov. 2002.

Chapter 4. Effect of Inflow Perturbations on Performance

Inflow disturbances can be caused by upstream fans, presence of upstream flow obstructions, by the presence of an upstream louver bank as in the case of automotive condensers and radiators, among other factors. In previous studies, the instability modes and characteristic frequencies in the louver bank have been identified. However, in all the geometries tested these modes appear at Re_{in} >700 for louver angles less than 40°. The objective of this study is to investigate whether inflow perturbations excite any of these modes for Re_{in} <500, and their effect, if any, on heat transfer coefficients. Table 4.1 summarizes the inlet flow conditions, which consist of a mean component (of unity) and a perturbation whose peak-to-peak amplitude (*a*) is varied from 0.1 to 1.0, and non-dimensional frequency (based on mean inlet velocity and louver pitch) which varies between 0.35 to 9.6.

Table 4.1: Summary of amplitude and frequency of inlet perturbations.

F_p = 1.5, θ =25˚, *Re* =300		F_p = 1.5, θ =25˚, *Re* =500		F_p = 2.0, θ =40˚, *Re* =500	
Amp. (a)	**Freq (f)**	**Amp. (a)**	**Freq (f)**	**Amp. (a)**	**Freq (f)**
	0.70	0.1	0.70	0.1	1.20
0.20	1.00		1.20		
	1.20			0.25	8.40
		0.5	0.70		
	0.70		1.20		0.70
0.5	1.00			0.50	1.20
	1.20	0.75	0.70		9.60
			1.20		
	0.70			0.75	0.70
0.75	1.00		0.07		1.20
	1.20		0.35		
		1.00	0.70		0.35
			1.20		0.70
			9.60	1.00	1.20
					4.80
					9.60
					24.0

Figure 4.1 shows the time-evolution of the heat transfer coefficient in the louver bank for two geometries at *Re*=500. In each calculation the inlet perturbation is superimposed on the mean flow at time=0 and the evolution of the heat transfer coefficient is monitored. At θ=25°, the unperturbed flow is steady, whereas at θ=40°, the unperturbed flow is unsteady. Over the range of parameter space tested, the results show that unless the amplitude of the perturbation is of the same order as the mean flow component and the frequency is high, inlet flow perturbations have very little effect on the heat transfer coefficient at low Reynolds numbers. Between the two geometries, the 40° geometry is more receptive to inlet perturbations.

Hence, from a practical viewpoint, it can be concluded that unless flow perturbations at the inlet to the heat exchanger are of the same order as the mean velocity component, any perturbations are quickly damped by the action of viscosity irrespective of frequency, and have very little effect on the heat transfer coefficient.

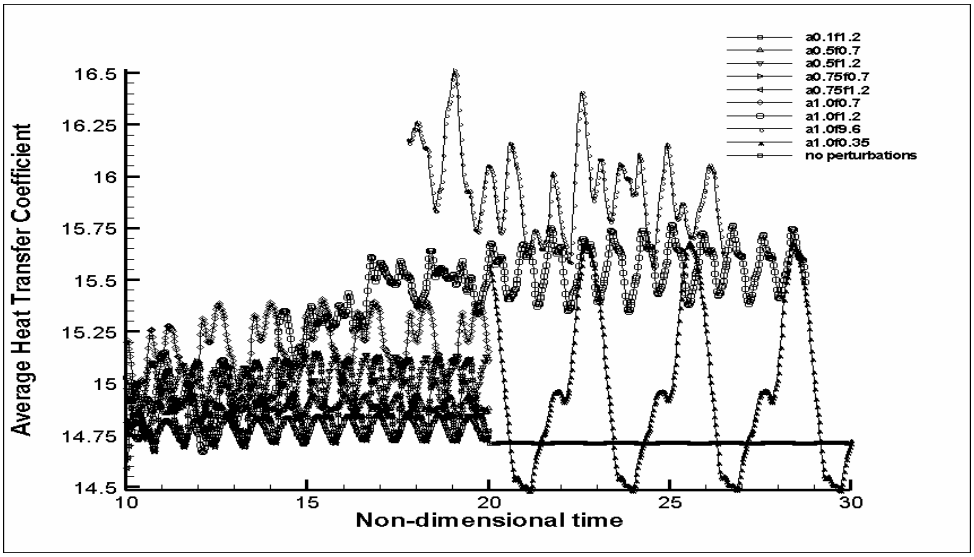

(a)

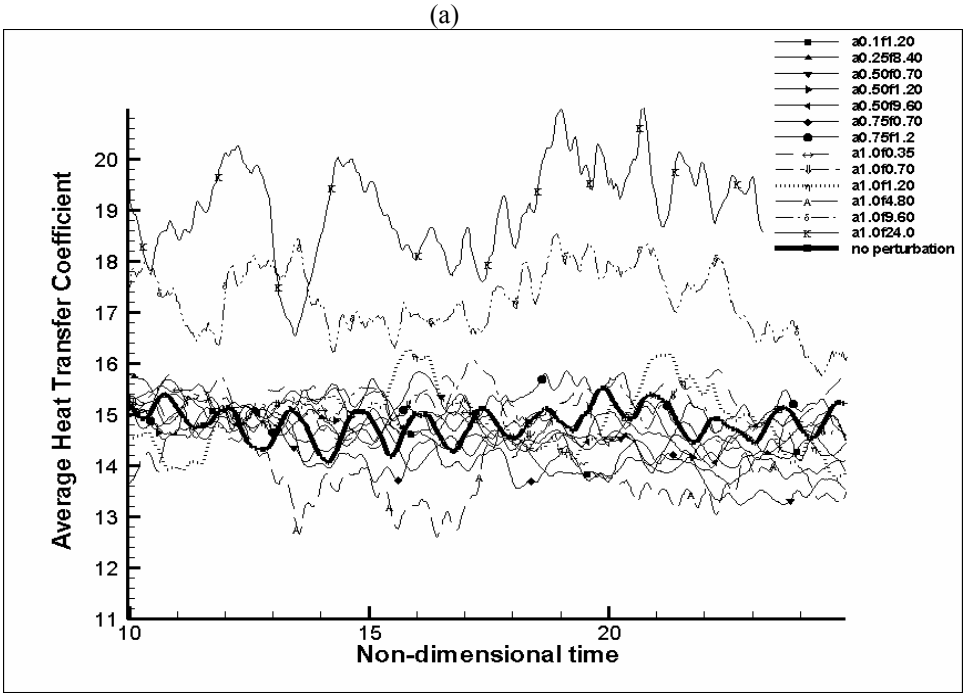

(b)

Figure 4.1: Heat Transfer Coefficients for (a) F_p =1.5, θ =25˚, Re=500; (b) F_p =2.0, θ =40˚, Re=500.